ACS APPLIED MATERIALS & INTERFACES

www.acsami.org

Research Article

Rapidly Gelled Lipoic Acid-Based Supramolecular Hydrogel for 3D Printing of Adhesive Bandage

Jiujiang Zeng, Haowei Fang, Haiyang Pan, Huijie Gu,* Kunxi Zhang,* and Yanli Song*

Cite This: *ACS Appl. Mater. Interfaces* 2024, 16, 53515−53531

Read Online

ACCESS | Metrics & More | Article Recommendations | Supporting Information

ABSTRACT: Developing a strongly adhesive, easily removable, and robust bandage is valuable in trauma emergencies. Poly(lipoic acid) (PLA)-based adhesives with good mechanical properties have been well-developed through a thermal ring-opening polymerization (ROP) method that is easiness. However, the additive manufacturing of PLA-based adhesives remains a challenge. Herein, α-lipoic acid (LA) and trometamol (Tris) are found to rapidly form a supramolecular hydrogel at room temperature with injectability and 3D printing potential. Meanwhile, the synthesized LA-grafted hyaluronic acid and cellulose nanocrystals are involved not only to optimize the extrusion of 3D printing but also to effectively promote fidelity and prevent the inverse closed-loop depolymerization of PLA in water. The hydrogel bandage exhibits strong adhesion to skin while it can be removed with no residue by water flushing, showing protection to neo-tissue during dressing replacement. The in vivo application of the hydrogel bandage significantly promoted wound healing by closing the wound, forming a physical barrier, and providing an anti-inflammatory effect, showing great potential in future clinical applications.

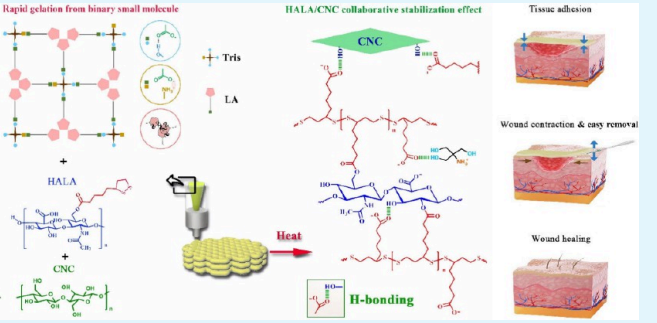

KEYWORDS: *α-lipoic acid, trometamol, supramolecular hydrogel, 3D printing, hydrogel adhesive*

1. INTRODUCTION

Skin injuries caused by disasters, wars, etc., are usually open wounds with uncontrolled bleeding, which has always been an important cause of death.[1] As the "gold standard" in clinical surgery, sutures, staples, and clips cannot be effectively applied outside the hospital. In addition, they will cause detrimental effects on the surrounding tissue and show limit in sealing wounds in friable tissues. Bioadhesives have been extensively studied for their ease of use and versatility as an alternative to sutures and staples.[2,3] For trauma first aid, the bioadhesives should exhibit high adhesive force to effectively close the wound, easy detachment for the subsequent therapies, and robust mechanical performance to form a physical barrier.[4,5] Adhesive hydrogels have received wide attention for their biocompatibility and biomimetic characteristics.[6] As the candidates for surgical sealants, they can form covalent bonding or noncovalent attractions to tissue surfaces.[7−10] At the same time, the enhanced mechanical performance not only provides a sufficient physical barrier to wounds but also acts as a supplement to interface adhesion to further promote adhesion strength.[11−13] In addition, like gauze, porous structure are more attractive for bandages because of their feature of absorbing wound exudate while maintaining breathability.[14,15] Thus, developing a strongly adhesive, easily removable, and robust porous hydrogel bandage is valuable for prehospital in trauma emergencies.

α-Lipoic acid (LA) is a small molecule coenzyme necessary for the aerobic metabolism of mitochondria and has natural biological safety. It has remarkable electrophilicity and the ability to react with free radicals and can eliminate superoxide and peroxide free radicals.[16] As an effective antioxidant, LA has been applied in clinics. Oxidation, heat, light, and mercaptan can trigger disulfide bond cleavage and exchange reactions in the dithiolane ring to initiate the ring-opening polymerization reaction to prepare poly(lipoic acid) (PLA),[17−19] which has been reported to possess reliable adhesion.[20] Adhesive preparations, including hydrogel adhesives preparation based on melting polymerization of LA, have been widely reported.[21−23] However, on the one hand, the currently reported LA polymerization methods mainly include thermal and light-stimulated polymerization, solvent volatilization-induced assembly polymerization, etc., which often require multiple operations or long duration. Huang et al. established deprotonation-promoted ring-opening polymerization of LA as a highly effective and simple method due to the long-range

Received: July 15, 2024
Revised: August 28, 2024
Accepted: September 17, 2024
Published: September 25, 2024

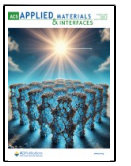

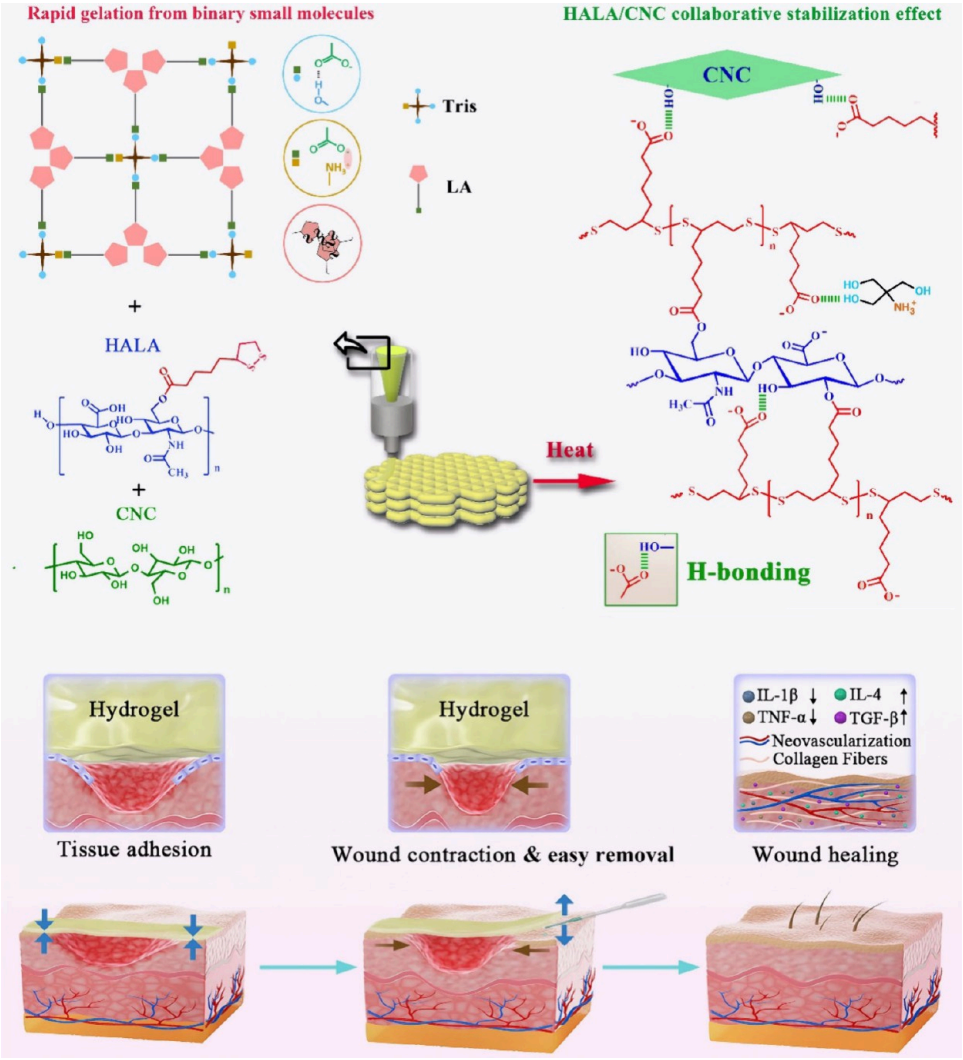

Figure 1. Schematic representation of hydrogel bandage preparation and functions. Formation of LA/Tris supramolecular hydrogel for molding and processing through 3D printing. Stabilization of PLA hydrogel was realized by HALA and CNC. The robust hydrogel bandage was used in wound healing to protect the wound and reduce inflammation.

electronic effect and nucleophilic carboxylate, which could be carried out at room temperature but also needed long duration.[24] Among these methods, it is difficult to find the right timing for 3D printing during the polymerization process. Once LA underwent effective polymerization, it normally has high viscosity and high adhesion to various substrates, which not only affect extrusion but also seriously interfere with path execution. Currently, only a few studies have developed fused deposition modeling (FDM) based on LA melt-polymerization or photopolymerization.[25−27] 3D printing of LA-based hydrogel bioadhesives has not been widely reported. Considering that 3D printing is advanced in the molding and processing,[28] especially in the manufacturing of bandages with porous structure, developing a new, general but simple approach for realizing 3D printing in the production of PLA-based hydrogel adhesives is significant but challenging.

On the other hand, the as-polymerized PLA-based supramolecular polymers are metastable due to the inverse ring-closing depolymerization, leading to adhesion failure of PLA-based adhesives. Although PLA-based supramolecular polymers can be stabilized by introducing multiple double-bond monomers, metal ions, ionic liquids, chlorinated organic solvent, etc.,[25,29,30] the unreacted small molecules are difficult to be removed, posing a biosafety concern for biomedical application.[21] Pioneer attempts have been recently made to stabilize PLA-based hydrogel bioadhesives by introducing polyphenols such as dopamine, tannin, etc., showing better biocompatibility and can be used for wound healing.[31,32] Nevertheless, the introduction of dopamine, tannin, etc., makes the removal of adhesives more complex.[33] Thus, it is urgent to develop biocompatible methods to effectively stabilize PLA-based adhesives with easy removal feature for biomedical applications.

Herein, LA was found to interact with trometamol (Tris) in water to rapidly form a binary supramolecular hydrogel at room temperature. Based on this, controllable 3D printing of the hydrogel adhesive was realized. At the same time, hyaluronic acid grafted with LA (HALA) was synthesized and employed as a macromolecular cross-linker to copolymerize with LA in the aqueous phase, with the presence of cellulose nanocrystals (CNC) as the giant physical cross-linker. For one thing, HALA and CNC associated with LA supramolecular hydrogel could optimize 3D printing. For another, HALA associated with CNC could prevent PLA

https://doi.org/10.1021/acsami.4c11704
ACS Appl. Mater. Interfaces 2024, 16, 53515−53531

chains from depolymerization by hydrogen bonding, leading to a long-term stabilized hydrogel adhesive. Besides, the presence of HALA endowed the hydrogel with higher cohesion and elasticity. Further introduction of cellulose nanocrystals (CNC) formed hydrogen bonds with PLA, endowing the hydrogel with robust features to withstand large deformation. The composite hydrogel bandage showed strong adhesion to different tissues and enhanced mechanical performances. More importantly, the hydrogel bandage could be removed with almost no residue by water flushing, showing protection to neo-tissue during dressing replacement (Figure 1).

2. MATERIALS AND METHODS

2.1. Materials. α-Lipoic acid (LA), trometamol (Tris), and 4-(dimethylamino)pyridine (DMAP) were purchased from Aladdin Biochemical Technology Co., Ltd. Hyaluronic acid (HA, $M_w = 4 \times 10^4$) was purchased from Bloomage BioTechnology Co., Ltd. Cellulose nanocrystals (CNCs) were purchased from ScienceK Co., Ltd. *N*,*N*′-Carbonyldiimidazole (CDI) was purchased from J&K Scientific Co., Ltd.

2.2. Preparation of LA/Tris Supramolecular Hydrogel. Tris was dissolved in distilled water at room temperature to prepare a 20% w/v solution. (The Tris solution at this concentration was used as the solvent in the present study.) LA was dissolved in Tris solution with the concentration of 50% w/v and stood for 5 min to yield a bulk hydrogel.

The rheological properties of the gelled LA-0 solution (LA 50% w/v, Tris 20% w/v) were tested using a rheometer (DHR-3, TA, USA) with a 12 mm flat steel plate fixture at room temperature. The gelled LA solution was placed onto the rheometer fixture and tested for its modulus−frequency relationship with a frequency sweep range of 0.01−100 Hz and a strain of 0.1%. Strain sweep measurements were carried out at a constant frequency of 1 Hz with strain ranging from 0.01 to 1000%. The viscosity change with the shear rate was continuously increased from 0.001 to 100 s^{-1} to evaluate their shear-thinning behavior.

The structure and binding energy of LA and Tris forming complexes were studied based on density functional theory (DFT). All calculations were performed by using the ORCA (version 6.0) program at the B3LYP-D3 and def2-SVP basis set levels for configuration optimization, while single point energy calculations were performed using the more accurate wB97M-V functional at the def2-TZVP level. All calculations were carried out under implicit water solvents (the conductor-like continuum polarization model (CPCM) and solvation models (SMD) have been implemented for water dissolution).[34−39] The binding energy of a compound could be calculated by the following formula:

$$E_{binding} = E_{L-T} - E_L - E_T \quad (1)$$

Among them, $E_{binding}$ was the single point energy of the complex formed by LA and Tris, while E_L and E_T were the individual single point energies of compounds LA and Tris.

A self-built and designed 3D bioprinting system was used for 3D printing. LA (50% w/v), HALA, and CNC were mixed in Tris solution (20% w/v) in a 5 mL syringe and placed at room temperature for 10 min to yield a bulk hydrogel. The stepper motor was used to drive the syringe plunger. The bulk hydrogel was printed from nozzles (from 18 to 21 G) at room temperature. The pneumatic pressure was 40 kPa. The printing speed was 10 mm/s, while the print path was generated by a numerical control system. After printing, the printed hydrogel was heated at 70 °C for 3 h for polymerization to yield a printed hydrogel.

2.3. PLA Adhesive Patch Preparation. Tris was dissolved in distilled water at room temperature to prepare a 20% w/v solution (the Tris solution at this concentration was used as the solvent in the present study). LA was added and fully dissolved in Tris solution to form a yellow and transparent solution, which was heated at 70 °C for 3 h and cooled to room temperature.

LA was dissolved in Tris solution to prepare solutions with different concentrations of 0.001, 0.01, 0.05, 0.1, 0.3, 0.5, 0.75, and 1 g/mL. After reacting at 70 °C for 6 h, the reactions were diluted to 0.001 g/mL. A UV spectrophotometer was employed to test the UV absorption spectra of LA at different concentrations.

A SmartLab intelligent diffractometer (XRD, Rigaku, Japan) was used to analyze LA and PLA. An appropriate amount of LA powder sample and a freeze-dried PLA solid sample was placed on a slotted flat glass sheet with gentle pressing. The crystal structure of the samples was measured. The scanning range of 2θ was 10°−90°, and the scanning speed was 10°/min.

The temperature-dependent rheological behavior of LA was tested at concentrations of 30% w/v. The three samples were subjected to temperature scanning using a rotary rheometer (DHR-3, TA, USA) with a 12 mm clamp. The strain was set to 1%, and the scanning frequency was maintained at 1 rad/s. The temperature scanning test was carried out at a heating rate of 1°/min between 10 and 90 °C.

2.4. PLA-HA-CNC Hydrogel Bandage Preparation. HALA was synthesized by grafting LA to HA via the esterification reaction according to our previous work.[40] HALA and LA were dissolved in Tris solution in sequence, followed by the addition of CNC to disperse evenly and heated at 70 °C for 3 h to prepare hydrogels, which were cooled to room temperature for study. The feeding conditions for the preparation of hydrogel are shown in Table 1.

Table 1. Feeding Conditions for the Preparation of Hydrogel

	component (mg)				solvent (mL)
sample	trometamol	HALA	CNC	LA	H_2O
PLA-HA1	200	10		500	1
PLA-HA2	200	20		500	1
PLA-HA-CNC3	200	20	30	500	1
PLA-HA-CNC5	200	20	50	500	1
PLA-HA-CNC7	200	20	70	500	1

TEM (JEM-200cx, JEOL, Japan) and DLS (ZS90, Marlven, British) were used to characterize the morphology, size, and zeta potential of CNC. FT-IR (NicoletiS10, Thermofischer, Germany) and DLS were used to characterize the interactions in the hydrogels. PLA-HA1, PLA-HA2, PLA-HA-CNC3, PLA-HA-CNC5, and PLA-HA-CNC7 precursors were prepared according to the feeding conditions in Table 1. The pH values of these precursors were measured by a pH meter (PHS-3TC, Shanghai). Then, the PLA-HA2, PLA-HA-CNC3, PLA-HA-CNC5, and PLA-HA-CNC7 hydrogels after gelling under the reaction conditions were immersed in distilled water for 4 h to record the pH value.

The storage modulus change during heating at 70 °C was monitored by a rheological test. The rapidly gelled LA(50% w/v)/Tris(20% w/v)/HALA(2% w/v)/CNC(5% w/v) was subjected to time scanning using a rotary rheometer (DHR-3, TA, USA) with a 12 mm clamp. The strain was set to 1%, and the scanning frequency was maintained at 1 rad/s. The temperature was 70 °C.

2.5. Lap-Shear Test. The surface of two glass slides was coated with 5% w/v gelatin solution with a coating size of 2.5 × 2.5 cm^2 after air drying for use. For the test of PLA adhesives, the PLA adhesives prepared from 30%, 40%, and 50% w/v LA solution were evenly spread on the gelatin-coated glass surface with an area size of 2.5 × 2.5 cm^2. For the test of PLA-HA1, PLA-HA2, PLA-HA-CNC3, PLA-HA-CNC5, and PLA-HA-CNC7 hydrogels, the hydrogels with the size of 2.0 × 1.0 × 0.5 cm^3 were adhered between the two gelatin-coated glasses. For the test of PLA-HA-CNC5 during removal, the PLA-HA-CNC hydrogels with a size of 2.0 × 1.0 × 0.5 cm^3 were adhered between the two gelatin-coated glasses, which were then immersed in water. After different durations, the glasses were subjected to the lap-shear test. The stretching rate in all lap-shear tests in this study was set as 50 mm/min.

https://doi.org/10.1021/acsami.4c11704
ACS Appl. Mater. Interfaces 2024, 16, 53515−53531

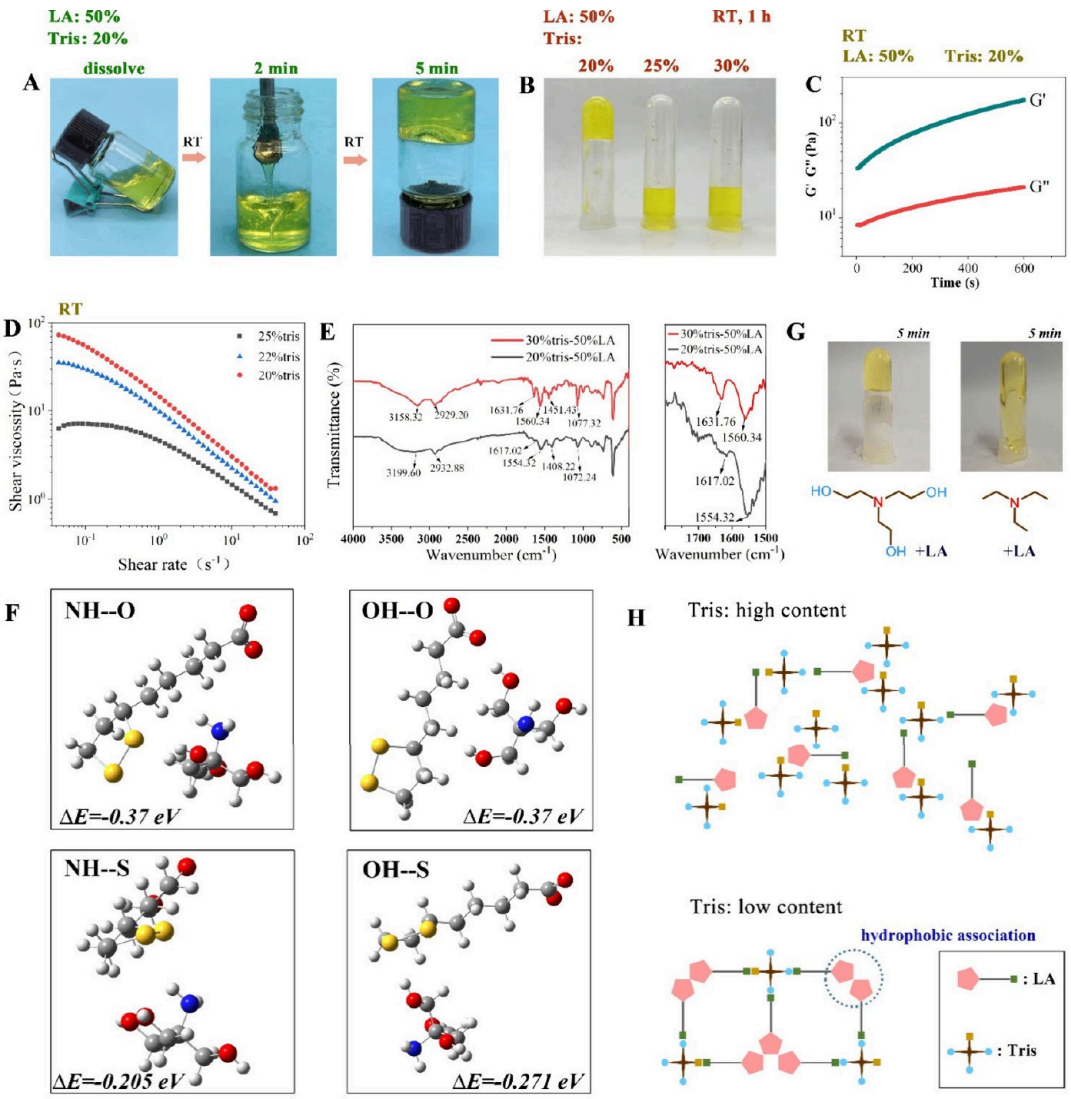

Figure 2. Rapid gelation from LA and Tris. (A, B) Effect of Tris concentration on gelation of the LA solution at room temperature. (C) Change of G' and G'' with time after LA dissolution (strain 1%, frequency 1 Hz, 25 °C). (D) Rheological testing of viscosity (strain 1%, 25 °C). (E) FT-IR spectra. (F) DFT simulation to illustrate the interaction between the O/S of LA with groups of Tris. (G) Mixing results were triethanolamine and triethylamine with LA. (H) Diagram of the mechanization of rapid gelation.

2.6. Self-Healing Test. The self-healing behavior of the hydrogel was evaluated by cyclic measurement of its storage modulus and loss modulus at 1% and 500% strain. Each test was carried out at a frequency of 1 Hz and a scanning time of 200 s.

2.7. Bursting Pressure Test. Gelatin solution (5 wt %) was prepared and applied evenly to the rubber tube that connected to the syringe. After air drying at room temperature, a hole with the diameter of 1 cm was created in the position where it was coated with gelatin. Then, the hydrogel with a thickness of 2 mm was adhered to cover the hole for 5 min for the measurement of the burst pressure. The peak pressure before pressure loss was considered as the burst pressure. After the hydrogel was blasted, it was kept for 5 min and then experienced the measurement for the second burst pressure. All measurements were repeated three times.

2.8. Swelling Behavior Test. Hydrogels (LA/Tris supramolecular hydrogel, bandage prepared after heating) were weighted and recorded (W_0), which were immersed in PBS to swell at different duration. After removing excess water, hydrogels were weighed and recorded (W_1), and then the swelling ratio (S_W) of the sample was calculated according to the following formula:

$$S_W = (W_1 - W_0)/W_0 \times 100\% \quad (2)$$

2.9. In Vitro Biocompatibility Test. Rat fibroblasts were purchased from Bluefbio Biology (Shanghai, China) and cultured in Dulbecco's Modified Eagle's medium (DMEM) with 10% fetal bovine serum (FBS) at 37 °C with 5% CO_2. Cells were seeded in 96-well plates and after 24 h. The hydrogel particles with the same weight were placed into wells (one per well) to co-culture with cells. A cell counting kit-8 (CCK-8, Dojindo, Japan) assay was used at 1, 3, 5, and 7 days after co-culture. The hydrogel particles and culture medium were removed, and the wells were washed 3 times with PBS. Then 10 μL of CCK-8 reagent was added into each well and incubated for 90 min. The absorbance was measured at 450 nm with a microplate reader (Tecan, Switzerland).

At the same time, the cell viability was observed by using a LIVE/DEAD viability/cytotoxicity kit (Beyotime, China). The hydrogel particles and culture medium were removed, and the wells were washed 3 times with PBS. The staining solution containing 1 μM calcein AM and 1 μM propidium iodide was added into the well, and the cells were incubated for 30 min at 37 °C in the dark. Live (green stain) and dead (red stain) cells were imaged by using an inverted fluorescence microscope (Carl Zeiss Meditec, Germany).

2.10. Mechanical Tests. The mechanical properties of the hydrogel were characterized by a rheological test. Cylindrical hydrogel

https://doi.org/10.1021/acsami.4c11704
ACS Appl. Mater. Interfaces 2024, 16, 53515−53531

samples were prepared with a diameter of 12 mm and a thickness of 5 mm and were placed on the center of the sample table of the rotary rheometer with a 12 mm clamp. The test was carried out at 25 °C using the frequency scanning mode (1% strain, 0.01−100 rad/s).

A dynamic thermomechanical analyzer (DMA 500) was employed for the compression tests. The cylindrical hydrogels with a diameter of 9 mm and a thickness of 5 mm were subjected to the compression test with a strain range of 0−100% to obtain the stress−strain curves. The compressive strength of the hydrogel sample referred to the stress of the sample at the fracture strain, which was recorded as δ_{max}. Compression moduli were calculated according to the following formula:

$$E = \frac{\delta_{10} - \delta_5}{\varepsilon_{10} - \varepsilon_5} \tag{3}$$

δ_5 and δ_{10} are the stress values of the hydrogel samples at the strain of 5% and 10%, respectively.

Hydrogel samples were then subjected to a cyclic compression test at room temperature. The cylindrical hydrogels were placed between the compression plate clamps of the dynamic thermomechanical analyzer. The compression rate and recovery rate were both 10%/min. After 20 cycles, the residual stress percentage was calculated according to the following formula:

$$\text{residual stress percentage } (\%) = \frac{\delta_{\text{max-20}}}{\delta_{\text{max-1}}} \times 100\% \tag{4}$$

Tensile tests were performed on hydrogel samples with the size of 20 × 10 × 2 mm^3 with a stretching rate of 10 mm/min on a universal testing machine (Instron-5943). The toughness was calculated from the area under the stress−strain curve. The universal testing machine (Instron 5943) was also used to carry out cyclic tensile tests on hydrogel samples with a cyclic tensile rate of 10 mm/min. The samples were restored to their original positions at the same rate. The energy dissipation of the hydrogel and the recoverable performance were recorded and calculated.

2.11. Wound Healing In Vivo. All the animal care, housing, and study procedures for rats complied with the ARRIVE guidelines and were performed in accordance with the National Research Council's Guide for the Care and Use of Laboratory Animals. The animal experiment was approved by The First Affiliated Hospital of Zhejiang University Ethics Committee (ZJ1H-2022-R-687). SD rats (male) were anesthetized by isoflurane gas, shaved, and washed with betadine.

For full-thickness wound repair, two circular full-layer wounds with a diameter of 10 mm were established on the dorsal axis of each rat. The metal rings were covered on the wounds and sutured with the surrounding skin to fix the wounds. The wound treated with a hydrogel bandage was employed as the Bandage group. The hydrogel bandage was changed on days 3, 5, 7, 9, 11, and 13 postsurgery. The wounds were washed with physiological saline to easily remove the old hydrogel bandages. The wound treated with hemostasis only was employed as the Blank group. A Simulated diagram of wounds was drawn by PowerPoint for area quantification. The proportion of the wound area was obtained according to the following formula:

$$\text{proportion of wound area} = \frac{S_t}{S_0} \times 100\% \tag{5}$$

S_0 represents the initial wound area on day 0, and S_t represents the wound area on day t.

Rats were sacrificed on day 7 and 14 for skin tissues collection (5 samples in each group). Samples were fixed with 4 wt % paraformaldehyde, embedded in paraffin, and sliced into pieces of 5 μm thickness. Then, the sections were histologically stained with H&E, Masson, and CD31 immunohistochemical staining. Meanwhile, another 5 rats were sacrificed on day 3 for skin tissues collection. Immunofluorescence staining was performed on samples on day 3 to detect the expression of IL-1β, TNF-α, IL-4, and TGF-β1 as well as the expression of iNOS and CD206. Fluorescence images were analyzed by ImageJ. A total of 15 rats were used in this model.

2.12. Statistical Analysis. Each measurement reported was based on a duplicate analysis of at least three independent experiments. The quantitative results were presented as mean ± SD. One-way analysis of variance (ANOVA) was used to reveal statistical differences, and $p < 0.05$ was considered statistically significant.

3. RESULTS AND DISCUSSION

3.1. Rapid Gelation from LA and Tris. Due to the poor solubility of LA in water, trometamol, as a weakly alkaline buffer component, is commonly used to achieve the dissolution of LA. In clinics, Tris is a commonly used buffer, which is usually used as an adjunct for LA injections. Although Tris is commonly used as a reagent for dissolving LA, its interaction with LA has rarely been rarely reported.

Interestingly, it was found in the present study that when the molar ratio of LA to Tris was in the range of 1.4−1.5:1, LA could rapidly gel within 5 min after dissolution at room temperature (Figure 2A). This effect of Tris on the rapid self-gelation of LA aqueous solution has been rarely reported. Reducing the dosage of Tris would make it difficult for LA to dissolve. Increasing the dosage of Tris would make LA more soluble, but gelation would not occur at room temperature (Figure 2B). In fact, the dissolution process of LA was a slow dissolution process with a small amount of multistep addition. When all LA was added, it had already shown an approximate solid state. Thus, as shown in Figure 2C, after LA total dissolution, the G' had been already higher than G''. In addition, there was a significant increase in G' at room temperature along with duration, confirming that the solution underwent a quick gelation during and after dissolution. Through the evaluation of the viscosity of LA solution (50% w/v) with different Tris content, it was found in Figure 2D that within the range of gelation molar ratio, LA solution quickly self-gelled to exhibit a viscosity significantly higher than that of LA solution (Tris concentration = 25% w/v). Of note, the molar ratio of LA to Tris (1.4−1.5:1) was broadly applicable for developing the rapid gelled hydrogels. However, to realize rapid gelation at room temperature, the LA concentration had to be higher than 30% w/v within the special molar ratio range. When the concentration of LA was lower than 30% w/v, the system still exhibited fluidity at a specific molar ratio. Reducing the amount of Tris would not produce rapid gelation but would lead to the reduction of the solubility of LA. Meanwhile, if the concentration was too high, the solubility of Tris in water would also significantly decrease, which was very difficult to maintain the special molar ratio. Therefore, this study evaluated the rapid gelation at the LA concentration of 10%−80% (through the vial inversion experiment after 10 min of preparation) and explained the range of components that could be rapidly gelled in Figure S1. In addition, G' of the rapidly gelled hydrogels increased with the increase of LA concentration. Besides, the rapidly gelled hydrogels immersed in a larger volume of water could swell with a swelling ratio over 3000% w/w but did not dissolve (Figure S2). However, they could slowly dissolved again in a larger volume of water with extra Tris, further confirming the key effect of Tris on the rapid gelation.

The mechanism for rapid gelation was further speculated. Since the content of Tris determined whether the system was gelated, it was speculated that under different Tris content, LA and Tris form different interactions, which might determine

https://doi.org/10.1021/acsami.4c11704
ACS Appl. Mater. Interfaces 2024, 16, 53515−53531

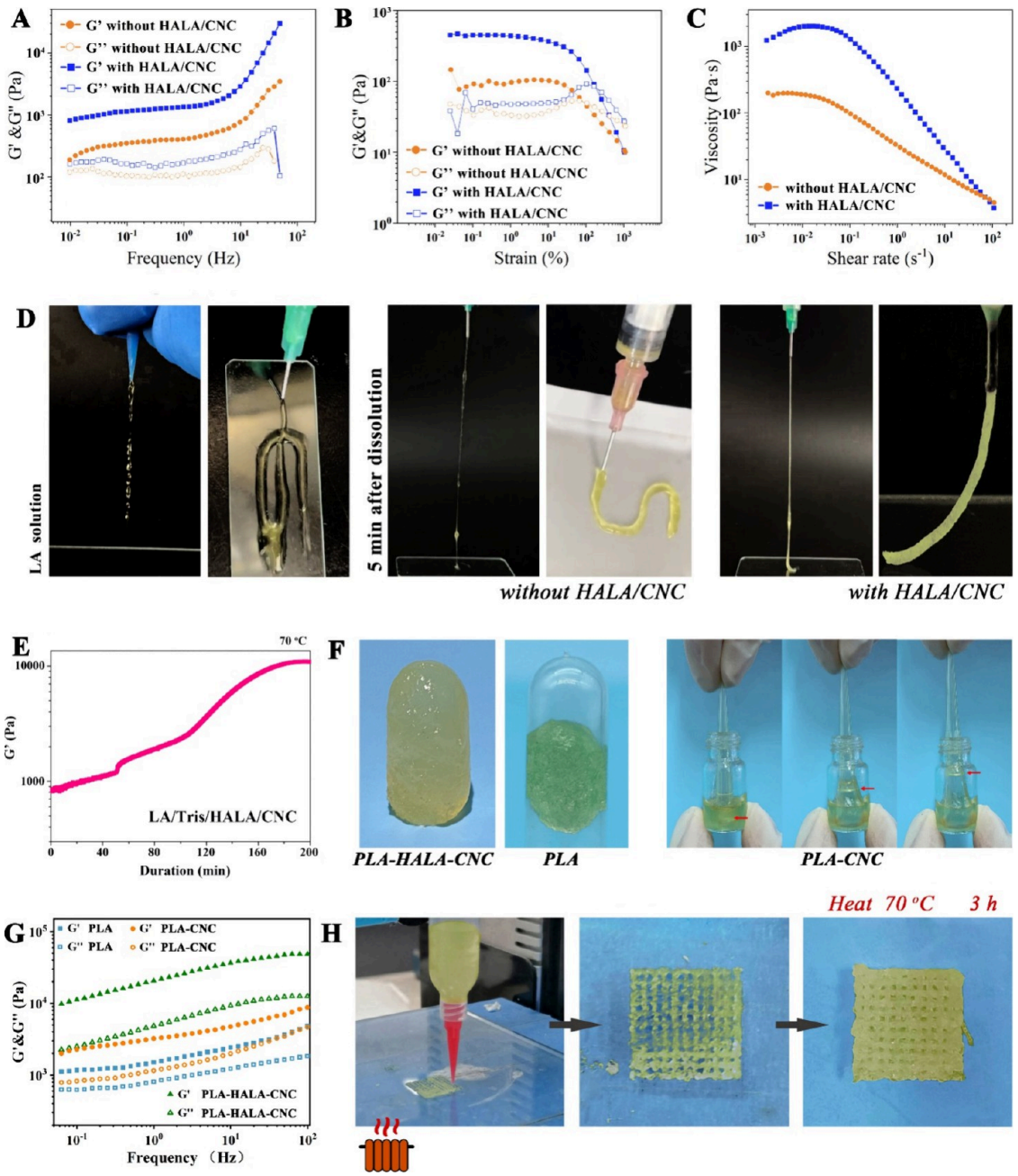

Figure 3. 3D printing protocol of PLA-based hydrogel. (A) Frequency scanning to evaluate the G' and G'' (strain 1%, 25 °C). (B) Strain scanning (frequency 1 Hz, 25 °C). The outliers at the beginning and end in (A) and (B) were more likely caused by the instrument. (C) Shear viscosity with increasing shear rates (strain 1%, 25 °C). (D) Images to show the extrusion of different inks. (E) G' change of the rapidly gelled LA/Tris/HALA/CNC during heating at 70 °C (strain 1%, frequency 1 Hz). (F) Appearance of PLA hydrogel with HALA/CNC, PLA hydrogel, and PLA hydrogel with CNC. The PLA-CNC hydrogel also was pastelike (red line indicated the bottom end of the lifting rod). (G) G' and G'' of the hydrogels after heating for polymerization (strain 1%, 25 °C). (H) 3D printing protocol demo.

whether the system was rapidly gelation. As shown in Figure 2E, for the LA solution with the concentration of 50% w/v, when the Tris concentration was 30% w/v, due to the deprotonation of the carboxyl group, the stretching vibration of the carboxyl group shifted to ~1560 cm^{-1}.[24] The absorption peak near ~1700 cm^{-1} corresponding to the stretching vibration of the carboxyl group of LA powder almost completely disappeared (Figure S3). More importantly, the characteristic vibrational absorption peak at ~1590 cm^{-1} belonging to the amino group of Tris (Figure S3) significantly shifted to ~1631 cm^{-1}, indicating that the characteristic absorption of the amino group changed after proton abstraction. However, when the Tris concentration was 20% w/v, the characteristic vibration absorption peak of the amino group shifted to 1617 cm^{-1}, indicating that the amino group was affected by a new interaction. Therefore, the interactions in the system showed significant differences with different concentrations of Tris. How this difference led to rapid gelation was further studied.

The structure and binding energy of LA and Tris forming complexes were studied based on density functional theory (DFT). As shown in Figure 2F and Table S1, both the O and S

https://doi.org/10.1021/acsami.4c11704
ACS Appl. Mater. Interfaces 2024, 16, 53515−53531

atoms in LA molecules could weakly interact with the amino and hydroxyl groups of the Tris molecule. The binding energy values between O and the amino/hydroxyl groups of Tris were greater than those between S and the amino/hydroxyl groups of Tris. LA can dissolve in organic alkaline solutions such as Tris, but it is worth noting that disulfide bonds are hydrophobic. Dithiolane containing hydrophobic disulfide bonds tend to aggregate in water.[41] However, DFT showed that the S atoms in the disulfide bond could form weak interactions with the amino and hydroxyl groups of Tris, which promoted the dispersion of hydrophobic dithiolane and facilitates the complete dissolution of LA. Therefore, when the Tris content was high, there will be excess Tris molecules that interact with the disulfide bonds of LA, promoting the dithiolane dispersion, thereby promoting the dissolution of LA in water. However, the interactions between disulfide bonds of LA and amino/hydroxyl groups of Tris was lower than the interactions between the O atoms of LA and amino/hydroxyl groups of Tris, indicating that the carboxylate group tended to preferentially interact with the protonated amino group and hydroxyl groups of Tris. Therefore, when the content of Tris was low, it is amino and hydroxyl groups that would preferentially bind to the deprotonated carboxyl groups of LA, forming a form of Tris molecule binding to multiple deprotonated carboxyl groups of LA. The dithiolane rings without Tris-binding in LA molecules were associated through hydrophobic interactions, thereby synergistically constructing a three-dimensional network structure with trometamol (Figure 2H).

Therefore, it was speculated that the rapid gelation of LA was dominated by the supramolecular interaction of LA and Tris at a certain molar ratio. Meanwhile, it was also difficult to deny that there was no ring-opening reaction of dithiolane in this process because at higher concentrations and hydrophobic aggregation of the dithiolane, the exchange reaction of disulfide bonds was possible. However, this reaction obviously did not dominate the rapid gelation at room temperature. Because at the same LA concentration (50% w/v), LA in 30% w/v Tris solution exhibited high fluidity without any signs of solidification. Effective LA polymerization typically requires high-temperature conditions to promote the reaction toward ring-opening polymerization. As shown in Figure S4, a solution containing 50% w/v of LA and 30% w/v of Tris exhibited a significant increase of G' only when it underwent long duration of heating. Therefore, it was speculated that this rapid gelation of LA at room temperature was not dominated by LA polymerization.

3.2. 3D Printing Protocol. Although PLA-based adhesives and PLA-based hydrogel adhesives have been widely reported recently, their molding methods are limited, which cannot meet the requirements of personalized, precise, fast, and high repeatability manufacturing. At present, the 3D printing of PLA-based hydrogels is rarely reported. This is closely related to the high viscosity of LA after polymerization, while the LA solution without polymerization cannot be used for 3D printing due to its fluidity. The rapid self-gelation of LA exhibited a significantly weaker adhesion before heating when compared to the polymerized hydrogel. Therefore, this study proposed a method based on the LA supramolecular hydrogel to realize 3D printing.

The rheological properties of the supramolecular hydrogels were further evaluated by rheological tests. In the frequency scanning mode, the rheological test showed that the G' of the rapidly gelled LA was greater than G'', confirming that it had the elasticity of bulk hydrogel (Figure 3A). At the same time, as shown in Figure 3B, the gelled LA was an elastic hydrogel under a small strain. While with the increase of the strain, G' began to decline and form an intersection with G''. The intersection point indicated that the hydrogel was broke under this strain, leading to a characteristic fluid transition. Therefore, with the shear strain increased, the gelled LA changed from the elastic solid state to the viscous flow state. This was closely related to the reversibility of supramolecular interactions. In addition, with the increase of shear rate, the viscosity of the gelled LA decreased, which indicated that it had the characteristic of shear thinning (Figure 3C). Such rheological properties made it possible for the gelled LA to be extruded. As shown in Figure 3D, the newly dissolved LA solution could be injected but did not have continuous extrudability due to its low viscosity, and there was no immediate plasticity after extrusion. After being placed at room temperature for 5 min, the extrudability of the gelled LA was significantly improved, enabling continuous extrusion and better plasticity after extrusion. However, the diameter of extruded filaments was significantly uneven with obvious extrusion swelling, which was still not meet the requirements for 3D printing.

To further optimize the printability, HALA and CNC were involved. The preparation and characterization of HALA and CNC are shown and discussed in Figures S5−S7 and Table S2. The introduction of HALA and CNC into LA solution (LA 50% w/v, Tris 20% w/v) would also lead to the same rapid gelation. The rheological behaviors of the gelled LA/HALA/CNC (LA: 50% w/v; trometamol: 20% w/v; HALA: 2% w/v; CNC: 5%) were similar to the gelled LA. G' of the gelled LA/HALA/CNC was higher than G'', indicating its elasticity. Meanwhile, G' values of the gelled LA/HALA/CNC were higher than those of the gelled LA, which was caused by the addition of HALA and CNC (Figure 3A). With the increase of strain, the G' of the gelled LA/HALA/CNC gradually decreased and was less than its G'' after reaching a certain strain, indicating that under a certain shear stress, the gelled LA/HALA/CNC changed from an elastic dominated solid state to a fluid state (Figure 3B). Similar to rapidly gelled LA, gelled LA/HALA/CNC also exhibited shear-thinning characteristics (Figure 3C). Although the failure stress and viscosity of gelled LA/HALA/CNC were increased due to the presence of HALA and CNC, the rheological evaluation results still supported that it had potential extrudability. As shown in Figure 3D, after being placed at room temperature for 5 min, the extrudability of the gelled LA/HALA/CNC was significantly improved, enabling continuous extrusion without significant extrusion swelling. At the same time, the extruded filament possessed better plasticity. The introduction of HALA and CNC significantly increased the viscosity of ink, which was beneficial for 3D printing including better continuity and self-supporting of extruded filaments. The more HALA and CNC there were, the higher was the printability of the ink (Figure S8). However, the amount of addition for both was limited. On the one hand, as the HALA content continued to increase, it became difficult to co-dissolve with high concentration LA/Tris solutions. On the other hand, excessive CNC content would affect the performance of printed bandages, which would be discussed later. Of note, the rapidly gelled LA/Tris supramolecular hydrogel was essential for realizing the 3D printing. As shown in Figure S8, ink (LA: 50% w/v;

https://doi.org/10.1021/acsami.4c11704
ACS Appl. Mater. Interfaces 2024, 16, 53515−53531

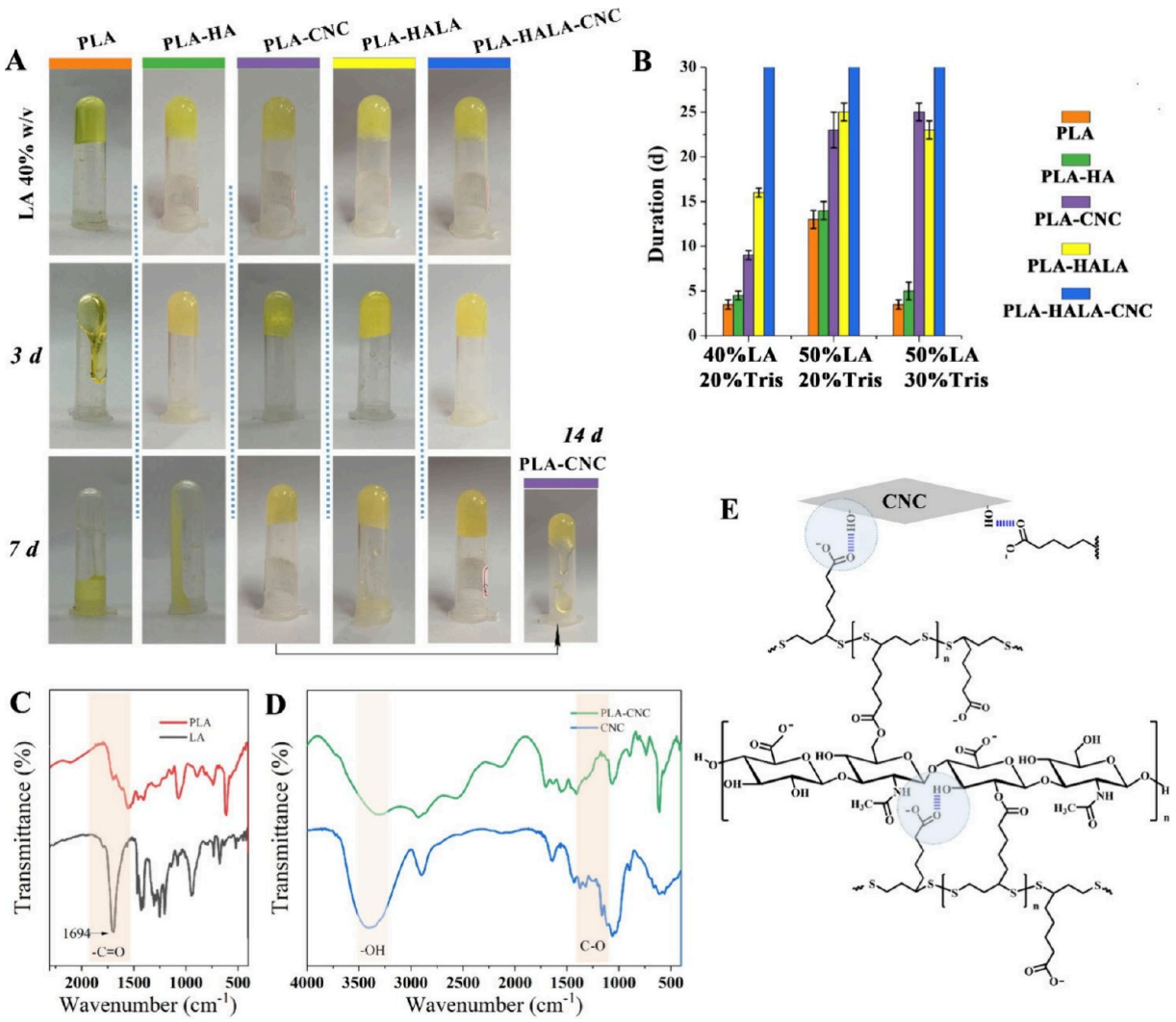

Figure 4. Effect of HALA and CNC on PLA stability. (A) Representative images to show the stability of PLA hydrogels (fabricated from 40% w/v LA) with different components. (B) Stability duration statistics. (C) FT-IR spectra of LA powder and PLA in solution. (D) FT-IR spectra of PLA and PLA-CNC. (E) Schematic representation of PLA-HA-CNC hydrogel network.

trometamol: 30% w/v; HALA: 2% w/v; CNC: 5%) was prepared from the nonrapidly gelled system as the comparison showed discontinuous extrusion and insufficient self-supporting. To improve the printability, it was necessary to rely entirely on other components (HALA and CNC), which was not feasible in this study.

Although the LA/Tris supramolecular hydrogel could be used for 3D printing, due to the limited interaction in the supramolecular hydrogels, their mechanical strength was weak, leading to another printing issue, fidelity. Previous studies have shown that ring-opening polymerization (ROP) of LA could be triggered by heating.[42] Similarly, in the aqueous phase, dissolved LA in the presence of HALA and CNC experienced ROP, with a significant increase in storage modulus (Figure 3E). The effect of LA concentration on the polymerization process was studied and is shown in Figure S9. The polymerized hydrogel after heating possessed a significantly enhanced self-support (Figure 3E). Of note, the presence of HALA and CNC not only optimized the extrusion of the ink but also ensured the stable plasticity and fidelity after polymerization. As shown in Figure 3F, given that there was no chemical cross-linking in PLA hydrogel, as well as PLA-CNC hydrogel, the weak hydrogen bonding made these two hydrogels like paste without formability after polymerization, which was not beneficial to the fidelity. However, the simultaneous participation of HALA and CNC endowed the hydrogel with improved fidelity. The G' of PLA-HALA-CNC hydrogel was significantly higher than that of PLA−CNC hydrogel and PLA hydrogel (Figure 3G). Based on these characteristics, the present study proposed a protocol for realizing 3D printing in the production of PLA-based hydrogel. As shown in Figure 3H, a LA/HALA/CNC solution was prepared in the printing material tank, followed by being placed at room temperature for 5−10 min, and then subjected for 3D printing of a porous dressing with a filament diameter of 500 μm and a filament gap of 500 μm. After printing, it was heated at 70 °C for 3 h for LA polymerization and stabilization to yield a more stable 3D printed hydrogel. However, according to statistics of filament diameter in Figure S10, during this process, the diameter of the extruded filament slightly increased, leading to the space between the filaments slightly decreasing after heating. For bandages, it was believed that the structure after heating still maintained a porous structure, which could meet the wound application require-

https://doi.org/10.1021/acsami.4c11704
ACS Appl. Mater. Interfaces 2024, 16, 53515−53531

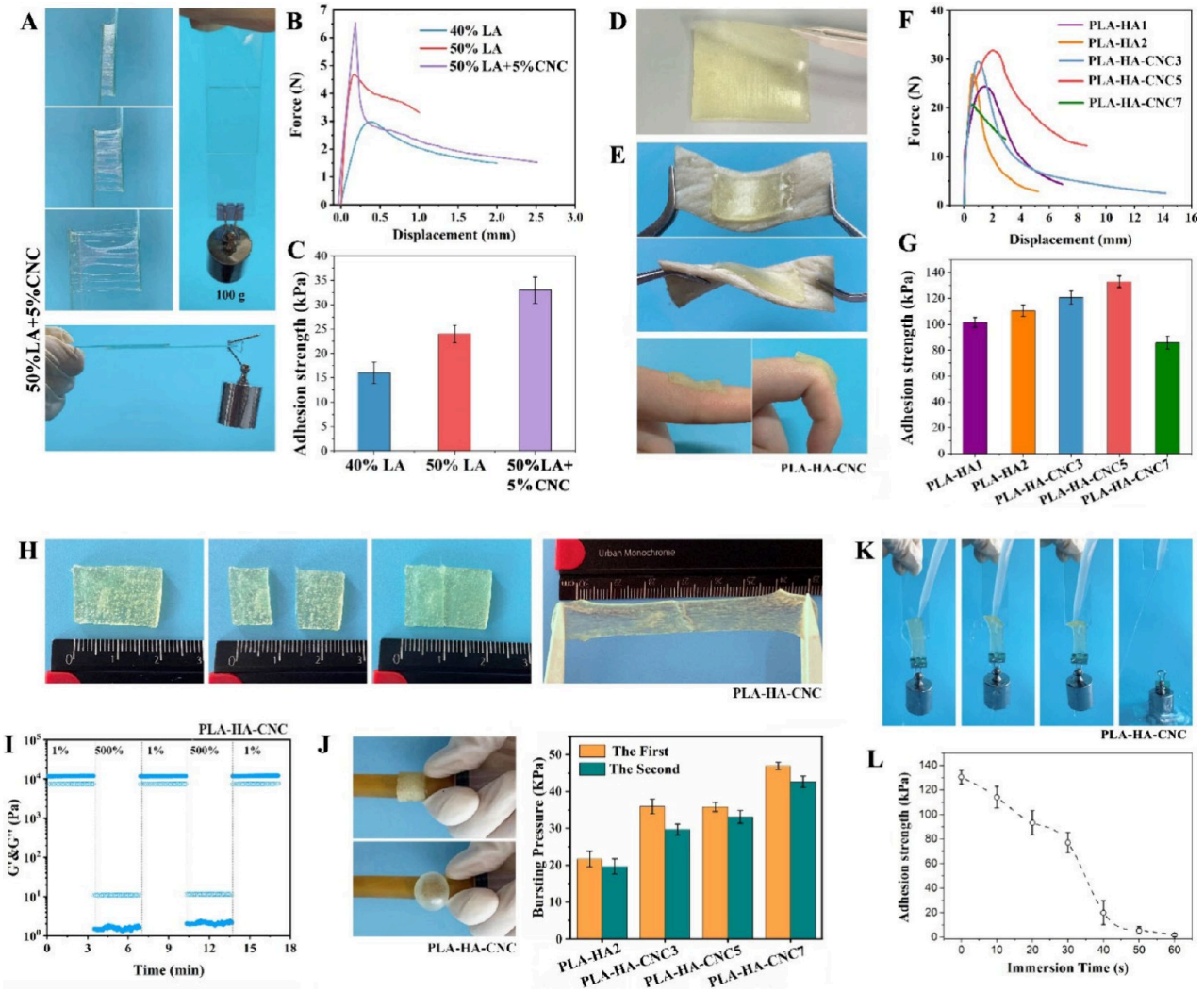

Figure 5. Adhesion and self-healing of the bandage after 3 h heating. (A) Images to show PLA-CNC adhered to two pieces of glasses coated with gelatin. (B) Lap-shear curves to show adhesion strength of PLA and PLA-CNC hydrogel adhesives (adhesion area = 2.5 cm × 2.5 cm). (C) Adhesion strength of PLA and PLA-CNC hydrogel adhesives. (D) Image to show the plastic PLA-HA-CNC hydrogel patch/bandage. (E) Images to show bandage PLA-HA-CNC adhered skin. (F) Lap-shear curves (adhesion area = 2.0 cm × 1.0 cm). (G) Adhesion strength. (H) Images showing the healing of the bandage PLA-HA-CNC. (I) Evaluation of self-healing of the bandage under alternating strains of 1% and 500%. (J) Images to show the burst pressure test and the burst pressure value (defined as the peak pressure before pressure loss). (K) Images showing the removal of the hydrogel bandage by water flushing. (L) Adhesion strength monitoring by lap-shear test.

ments of breathability. Thus, the influence of Tris on LA gelation and the positive influence of HALA and CNC on the rheological properties and extrudability of the ink realized and optimized the molding and processing of PLA-based hydrogels through 3D printing.

3.3. Effect of HALA/CNC on PLA Stability. After the molding of the PLA hydrogel, the stability of the PLA hydrogel was another important issue that needed to be focused on. The ROP of LA led to the alternative existence of disulfide bonds in the main chain, thus forming a linear polymer. However, because of the presence of thiol radicals, PLA could not remain stable after falling to room temperature and would depolymerize into oligomers, resulting in a decrease in viscosity and exhibiting fluidity.[21] The depolymerization of PLA would significantly affect its performance. In order to study the influence of the introduction of HA, HALA, and CNC on the stability of PLA, hydrogels with different compositions, including PLA, PLA-HA, PLA-CNC, PLA-HALA, and PLA-HALA-CNC, were prepared by heating. The stability of hydrogels was observed by an inversion experiment at room temperature. As shown in Figure 4A, the bulk hydrogels (fabricated from 40% w/v LA) with different components formed by heating polymerization could stably exist at the bottom of the centrifuge tube when it was inverted. However, after 3 days at room temperature, due to depolymerization, PLA became a flowable liquid and flowed down under gravity. But other hydrogels remained stable at 3 days. After 7 days, the PLA-HA hydrogel also underwent obvious phase transformation and became a liquid, revealing the significant depolymerization. The other hydrogels did not undergo an obvious phase transformation. PLA-CNC showed significant fluidity after 9 days, while PLA-HALA showed significant fluidity after 14 days. Both CNC and HALA showed significantly positive effect on stabilizing PLA. The present study continued to extend the observation time and finally found that the PLA-HALA-CNC hydrogel was the most stable and did not undergo obvious depolymerization during the 4-weeks observation duration. Further statistics were carried out

https://doi.org/10.1021/acsami.4c11704
ACS Appl. Mater. Interfaces 2024, 16, 53515−53531

on the stability of hydrogels with different compositions (Figure 4B). For the PLA hydrogel fabricated from 50% LA, the effect of CNC on stabilizing PLA was more significant. The contributions of CNC and HALA to the stability of PLA was similar. The results confirmed that the introduction of either CNC or HALA could significantly improve the stability of PLA, so that the polymerized hydrogel could maintain a solid state for a long time and show elasticity. Collaboration between CNC and HALA could better stabilize PLA. HA could also improve the stability of PLA, but this effect seemed weak.

Accordingly, the terminal sulfur radicals of PLA initiate the reverse ring-closing depolymerization and revert to monomers after cooling, attesting to a more thermodynamically stable LA monomer.[21,30] Thus, strategies such as the introduction of 1,3-diisopropenylbenzene (DIB) and chlorinated solvents, etc. were used to stabilize PLA by quenching the terminal sulfur radicals.[24] At the same time, 1-ethyl-3-methylimidazolium ethyl sulfate ([EMI][ES]) and the deprotonated LA monomer, etc., were also used to form hydrogen bonds with PLA to lower the potential energy of PLA, thus stabilizing PLA.[30] In this study, FT-IR was used to illustrate the possible mechanisms. As shown in Figure 4C, the sharp absorption peak at 1702 cm^{-1} corresponding to the stretching vibration of the carboxyl group shifted to 1545 cm^{-1}, indicating that carboxyl groups in PLA were deprotonated in Tris aqueous solution.[21] For the PLA-CNC hydrogel, the O−H stretching vibration peak at 3400 cm^{-1} underwent a significant red shift, and the C−O stretching vibration peaks in the 1000−1300 cm^{-1} region also changed, confirming the formation of H-bonding between the hydroxyl groups of CNC as H donors and the $-COO^-$ of PLA (Figure 4D). In addition, the zeta potential of CNC was -57.53 ± 1.67 mV, which dropped to -11.22 ± 1.68 mV after the interaction with LA in solution. The reduction of negative charges indicated that the hydroxyl groups of CNC were shielded due to their interaction with the $-COO^-$ (Figure S11). At the same time, HALA acted as the macromolecular cross-linking agent that could achieve network formation of PLA and reduce the efficiency of sulfur radicals reaction, significantly improving PLA stability (Figure 4E).

Thus, HALA and CNC synergistically improved the stability of PLA, allowing it to maintain long-term stability even in a low-temperature storage environment of 4 °C. The improvement of PLA stability is significant for maintenance of its function.

3.4. Adhesion and Self-Healing Performance of Hydrogel Bandage. According to the above research results, the PLA-based hydrogel in this study could be produced by 3D printing and had reliable stability after heating. Then, its adhesion as a bioadhesive was evaluated next. In order to study the adhesion of the present PLA-based hydrogel, PLA-based hydrogel patches after 3 h heating without complex structure were prepared. Due to a large number of carboxyl groups, PLA has been reported to have adhesive ability.[21] As shown in Figure 5A−C, the PLA-CNC hydrogel also showed adhesion performance. It was capable of tightly bonding two glass sheets coated with gelatin. Two glass sheets bonded by the PLA-CNC hydrogel could withstand a weight of 100 g. When the two glass sheets were pulled apart, the adhesive still firmly adhered to them, but the adhesive itself was damaged, confirming that the adhesive had strong interfacial adhesion. According to lap-shear tests, the adhesion strength increased with the increase in LA concentration. In addition, the presence of CNC formed hydrogen bonding with PLA, promoting the cohesion, leading to the promotion of adhesion strength. The failure of adhesion mainly lied in the destruction of hydrogel adhesive, which was obviously related to the low cohesion of the adhesive. Because of the absence of chemical cross-linking in PLA hydrogel adhesive and PLA-CNC hydrogel adhesive, these two groups of hydrogel adhesives were paste-like without formability.

The presence of HALA could make up for this deficiency. The presence of HALA could not only significantly improve the stability of PLA but also improve the cohesion and strength of hydrogel bandages through the formation of covalent cross-linking. As shown in Figure 5D and Figure S12, the PLA-HA-CNC hydrogel could be molded to form a patch or a bandage. The PLA-HA-CNC hydrogel could firmly adhere to the skin surface and could twist with the skin twisting without falling off (Figure 5E). The lap-shear test showed that the adhesion strength of PLA-HA1 (PLA: 50% w/v; HALA: 1% w/v), PLA-HA2 (PLA: 50% w/v; HALA: 2% w/v), PLA-HA-CNC3 (PLA: 50% w/v; HALA: 2% w/v; CNC: 3%), PLA-HA-CNC5 (PLA: 50% w/v; HALA: 2% w/v; CNC: 5%), and PLA-HA-CNC7 (PLA: 50% w/v; HALA: 2% w/v; CNC: 7%) hydrogel bandages was ∼102−111, ∼122, ∼134, and ∼83 kPa, respectively (Figure 5F,G). The adhesion strength increased with the increase of the HALA content and the CNC content. However, excessive CNC content significantly reduced the adhesion strength of the PLA-HA-CNC bandage. The presence of CNC formed hydrogen bonding with the carboxyl groups of PLA, which consumed the carboxyl content in the hydrogel network, thus reducing the effective groups interacting with the tissues. FibrinGlue (Porcine Fibrin Sealant Kit, BIOSEAL BIOTECH CO., Ltd.) was used as the control adhesive and underwent the same lap-shear test. The adhesion strength of FibrinGlue was ∼12 kPa. Thus, the hydrogel bandages showed significantly higher adhesion than the clinic used FibrinGlue.

Due to the strong adhesion, the two cut hydrogel bandages could instantly adhere and heal immediately after contact immediately. And the healing was firm, which could withstand large tensile deformation without fracture (Figure 5H). High and low cyclic strain tests had also confirmed that the hydrogel bandage had an excellent self-healing performance (Figure 5I). After two cycles of alternating strain, the storage modulus and loss modulus of hydrogel bandage could be almost completely recovered. Based on the strong adhesion and self-healing properties, the performance of the hydrogel bandage in the burst pressure test was impressive. As shown in Figure 5J, a long cut of 1 cm was made on the rubber tube, plugged at one end. The cut was blocked with the hydrogel bandage. It was found that the hydrogel bandage was closely attached to the rubber tube. With the injection of air, the hydrogel bandage expanded like a balloon due to pressure until it broke. The average bursting pressure of PLA-HA2, PLA-HA-CNC3, PLA-HA-CNC5, and PLA-HA-CNC7 hydrogel bandages were ∼21.67, ∼36, ∼35, and ∼47 kPa, respectively. After the fracture, the hydrogel bandage still adhered tightly to the rubber tube. Because of the excellent self-healing performance of the hydrogel bandage, the second test was carried out immediately within 5 s after the fracture, and the bursting pressure of the hydrogel bandage still reached 80%−95% of the original bursting pressure.

3.5. Bandage Removal and Re-adhesion. Usually, in clinical applications, dressings need to be replaced regularly.[43] Excellent adhesion performance may also lead to another

https://doi.org/10.1021/acsami.4c11704
ACS Appl. Mater. Interfaces 2024, 16, 53515−53531

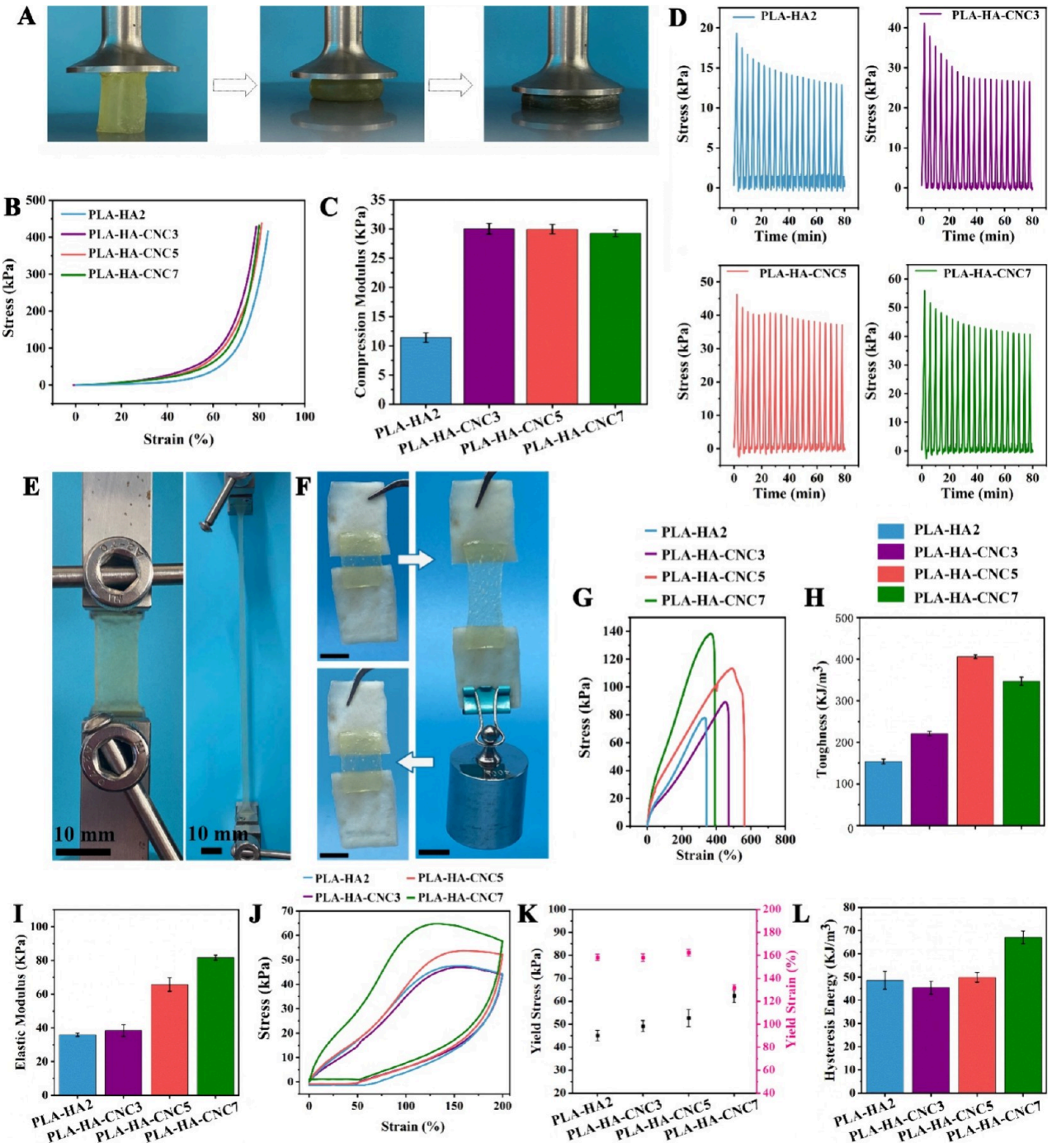

Figure 6. Mechanical performance of hydrogel bandages after 3 h heating. (A) Images to show the cylindrical hydrogel under compression. (B) Compressive stress−strain curves. (C) Compression modulus of hydrogels. (D) Stress−time curves of hydrogels in the cyclic compression test. (E) Images to show hydrogel bandage deformation in the tensile test. (F) Images to show hydrogel bandage adhered on two pig skins with loading and unloading of external force. (G) Tensile stress−strain curves. (H) Toughness of hydrogels. (I) Young's moduli of hydrogels. (J) Tensile stress−strain curves in the cyclic tensile test. (K) Yield stress and yield strain of hydrogel in the cyclic tensile test. (L) Hysteresis energy of hydrogels in the cyclic tensile test.

challenge, which is the difficulty of separating and removing the material from the adhesive site, leading to secondary damage to the wound. How to achieve simple and residue-free removal is crucial for wound healing in the clinic. There are different methods for removing adhesives based on different adhesion mechanisms, such as rapidly degrading adhesives and reducing the interfacial adhesion between adhesives and tissues through competitive reactions.[43] However, small molecules or ions are usually involved, which may bring potential risks.

In the present study, although the hydrogel bandage possessed excellent adhesion, it could be removed without a residue. As shown in Figure 5K, the adhesion between hydrogel bandage (PLA-HA-CNC5) and substrate could be significantly reduced by using water washing, thus realizing the detachment of the hydrogel bandage with almost no residual.

https://doi.org/10.1021/acsami.4c11704
ACS Appl. Mater. Interfaces 2024, 16, 53515−53531

According to the monitoring of the adhesion strength, it was found that the adhesion strength reduced to ∼0 kPa within 60 s (Figure 5L). As shown in Figure S13, the prepared bandage immersed in water showed quick water adsorbing. Although there was no significant change in shape and volume within 60 s, the swelling test showed that the bandage had a significant binding with water within 60 s after contact with water. This was mainly due to a large number of dense carboxyl groups and HA in hydrogel bandage that could absorb water molecules to form a hydration layer at the interface, which would destroy the binding force between hydrogel and substrate. Water would affect the adhesion of the hydrogel bandage, but according to the monitoring of the adhesion strength in Figure 5L, a small amount of water would not affect the stable adhesion of the hydrogel bandage on the substrates. The complete desorption process required a considerable amount of water. Besides, after drying at 37 °C for 30 min, the removed hydrogel bandage could restore its adhesion. However, the adhesion strength decreased with an increase in adhesion−detachment times (Figure S14).

3.6. Mechanical Performance of the Hydrogel Bandage. Generally, hydrogels exhibit soft and weak or hard and brittle mechanical properties. As a wound bandage for first aid of trauma, hydrogels should exhibit mechanical performance similar to skin to adapt to activities at different parts. Thus, the mechanical performance of the hydrogel bandages after 3 h heating was evaluated.

Compression tests showed that the cylindrical hydrogel could be largely deformed to withstand extreme compression without being destroyed (Figure 6A). Consistent with rheology tests, the compression modulus significantly improved with the addition of CNC (Figure 6B,C). At the same time, the antifatigue properties of the hydrogels were evaluated by compression cycling test. As shown in Figure 6D, after the first cycle, the stress of the hydrogels showed a downward trend, but with the increase in cycle times, the mechanical properties of the hydrogels tended to be stable. The average residual stress percentages of the hydrogel PLA-HA2, PLA-HA-CNC3, PLA-HA-CNC5, and PLA-HA-CNC7 after 20 cycles of compression were ∼70%, ∼70%, ∼86%, and ∼80%, respectively (Figure S15). The compression tests showed that the hydrogels exhibited typical viscoelasticity dominated by elasticity. They could not fully recover but partially recover after the external force was removed. However, compared with PLA-HA hydrogel, the addition of CNC provided more interactions with PLA, reducing stress loss during cyclic testing and thus promoting the elasticity of hydrogels.

Tensile tests further showed that the hydrogel bandage could be stretched to a high deformation (Figure 6E). As shown in Figure 6F, two separated pig skin pieces were adhered by the hydrogel PLA-HA-CNC3. A 100 g weight was hung on one skin piece to exert a loading stress. It was found that the hydrogel tightly adhered to the pig skins and stretched to large deformation under the action of external force. After removing the external force, the hydrogel shrunk rapidly with most of the deformation restored. The fracture strain of hydrogel PLA-HA2, PLA-HA-CNC3, PLA-HA-CNC5, and PLA-HA-CNC7 was ∼348%, ∼476%, ∼565%, and ∼396%, respectively (Figure 6G). Through calculation, the toughness of hydrogel PLA-HA2, PLA-HA-CNC3, PLA-HA-CNC5, and PLA-HA-CNC7 was 153.75 ± 5.66, 220.79 ± 5.38, 406.04 ± 4.63, and 347.05 ± 9.86 kJ/m^3, respectively (Figure 6H). The Young's modulus of hydrogel PLA-HA2, PLA-HA-CNC3, PLA-HA-CNC5, and PLA-HA-CNC7 was 35.96 ± 1, 38.43 ± 3.52, 65.72 ± 4.13, and 81.71 ± 1.46 kPa, respectively (Figure 6I). Of note, the presence of CNC significantly improved the modulus and the fracture strain of hydrogel. This was mainly attributed to the extensive hydrogen bonding between CNC and PLA. For one thing, nanoparticles filling and the hydrogen bonding promoted the modulus of hydrogels.[18] For another, under the action of an external force, these hydrogen bonds were destroyed, which dissipated the external force and enabled the hydrogel to withstand large deformation. However, the fracture strain of the hydrogel PLA-HA-CNC7 decreased when compared with the hydrogel PLA-HA-CNC5, which might be related to the uneven dispersion of CNC at high concentration.

The test of loading and unloading stress was further carried out to study the deformation recovery of hydrogel bandages under tensile mode. The cyclic tensile testing of the hydrogel showed that the hydrogels had obvious hysteresis after the loading and unloading cycles at 200% strain (Figure 6J). The yield stress of hydrogel PLA-HA2, PLA-HA-CNC3, PLA-HA-CNC5, and PLA-HA-CNC7 was 45.12 ± 2.25, 49.25 ± 2.35, 52.64 ± 3.72, and 62.4 ± 2.89 kPa, respectively. The yield strain of hydrogel PLA-HA2, PLA-HA-CNC3, PLA-HA-CNC5, and PLA-HA-CNC7 was 158.24 ± 2.7%, 158.16 ± 3.15%, 162.43 ± 2.82%, and 131.89 ± 2.52%, respectively (Figure 6K). Through calculation, the hysteresis energy of hydrogel PLA-HA2, PLA-HA-CNC3, PLA-HA-CNC5, and PLA-HA-CNC7 was 48.57 ± 3.79, 45.38 ± 2.76, 49.83 ± 2.05, and 67.06 ± 2.73 kPa, respectively (Figure 6L). The mechanical tests thus illustrated that the hydrogel bandages were robust to withstand and adapt to external forces, so as to provide a more stable and sufficient protective barrier to wounds.

3.7. Application of 3D Printed Porous Hydrogel Bandage in Full-Thickness Skin Wounds. Before being used in vivo, the biosafety of the hydrogel without any post-treatment was first evaluated. Of note, the prepared hydrogel bandages without postprocessing possessed a pH value close to neutral (Figure S16). Moreover, the hydrogel bandage, PLA-HA-CNC5, co-cultured with fibroblasts showed no significant cytotoxicity. Almost no dead cells were observed during the 7 day culture (Figure S17). Cells kept proliferation during the in vitro co-culture and showed no significant difference with the control group, revealing the safety and biocompatibility of the hydrogel bandage. Normally, to ensure biocompatibility, it is necessary to remove small molecules and cross-linking agents that have potential cytotoxicity in the preparation process of adhesive hydrogels. However, LA is a co-enzyme involved in acyl transfer in the metabolism of substances in the body, which can eliminate free radicals that lead to accelerated aging and disease. Low concentrations do not cause toxicity.[44] At the same time, HA and CNC also have excellent biocompatibility.[40,45] Therefore, the hydrogel formed by the polymerization of LA as the monomer could be used without post-treatment. This reduced the technical and equipment thresholds of hydrogel bandage preparation and greatly improved the generalization of hydrogel bandage preparation.

Considering its well-performed adhesion, robust feature, and biocompatibility, hydrogel PLA-HA-CNC5 was used to treat wounds. The porous hydrogel bandage was prepared by 3D printing, possessing a filament diameter of 300 μm and a filament gap of 400 μm for providing better breathability to

https://doi.org/10.1021/acsami.4c11704
ACS Appl. Mater. Interfaces 2024, 16, 53515−53531

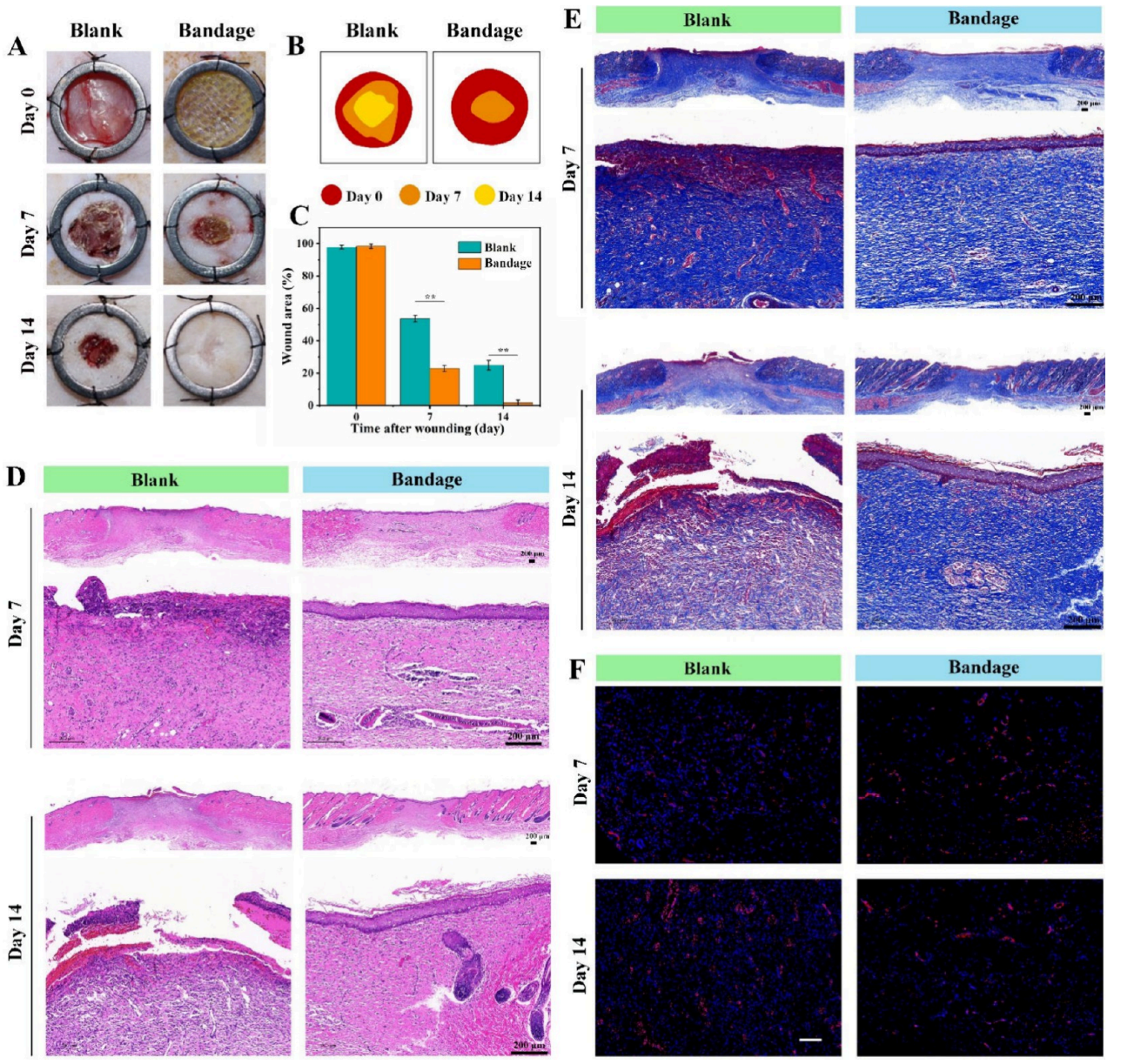

Figure 7. Healing of full-thickness skin wounds. (A) Images to show wounds on day 0, 7, and 14 postsurgery in the Blank group and the Bandage group. (B) Simulated diagram of wound healing. (C) Quantification of wound residual area rate (**$p < 0.01$). (D) H&E staining of the wounds on day 7 and 14 postsurgery in the Blank group and the Bandage group (bar scale: 200 μm). (E) Masson staining of the wounds on day 7 and 14 postsurgery in the Blank group and the Bandage group (bar scale: 200 μm). (F) CD31 immunofluorescence staining of the wounds on day 7 and 14 postsurgery in the Blank group and the Bandage group (bar scale: 100 μm). $n = 5$.

larger wounds. As shown in Figure 7A−C, compared with the Blank group, the healing rate of skin wounds in the Bandage group was significantly faster on day 7. The wound residual area in the Bandage group reduced to ∼20% on day 7, which was much lower than that in the Blank group (∼55%). After 14 days, the wounds treated by hydrogel bandage PLA-HA-CNC5 were completely healed, exhibiting a similar color and texture to normal skin. However, more than 20% of the wounds had not been healed in the Blank group on day 14.

H&E staining and Masson staining were performed to further study the effect of the hydrogel bandage on wound healing. As shown in Figure 7D,E, neo-tissues were observed in both the Blank group and Bandage group. The epidermis in the regenerated area of the Bandage group was found to be continuous on day 7. Complete squamous epithelial tissue could be observed. However, the epidermis in the Blank group was not observed. According to Masson staining, collagen deposition could be observed in the two groups. While collagen in the Bandage group showed regular arrangement. After 14 days, the epidermis could be observed in the Blank group, which, however, was still discontinuous. In the Bandage group, the wounds further contracted and healed. The collagen fibers in the Bandage group were thicker and denser, with a more mature phenotype and regular orientation. The Blank group had the least deposition and loose arrangement of collagen fibers. The histological results were consistent with the general observation. In addition, angiogenesis was further monitored. Angiogenesis can continuously provide sufficient oxygen and nutrients to the wound.[46] According to the staining of CD31, a common indicator to characterize vascular

https://doi.org/10.1021/acsami.4c11704
ACS Appl. Mater. Interfaces 2024, 16, 53515−53531

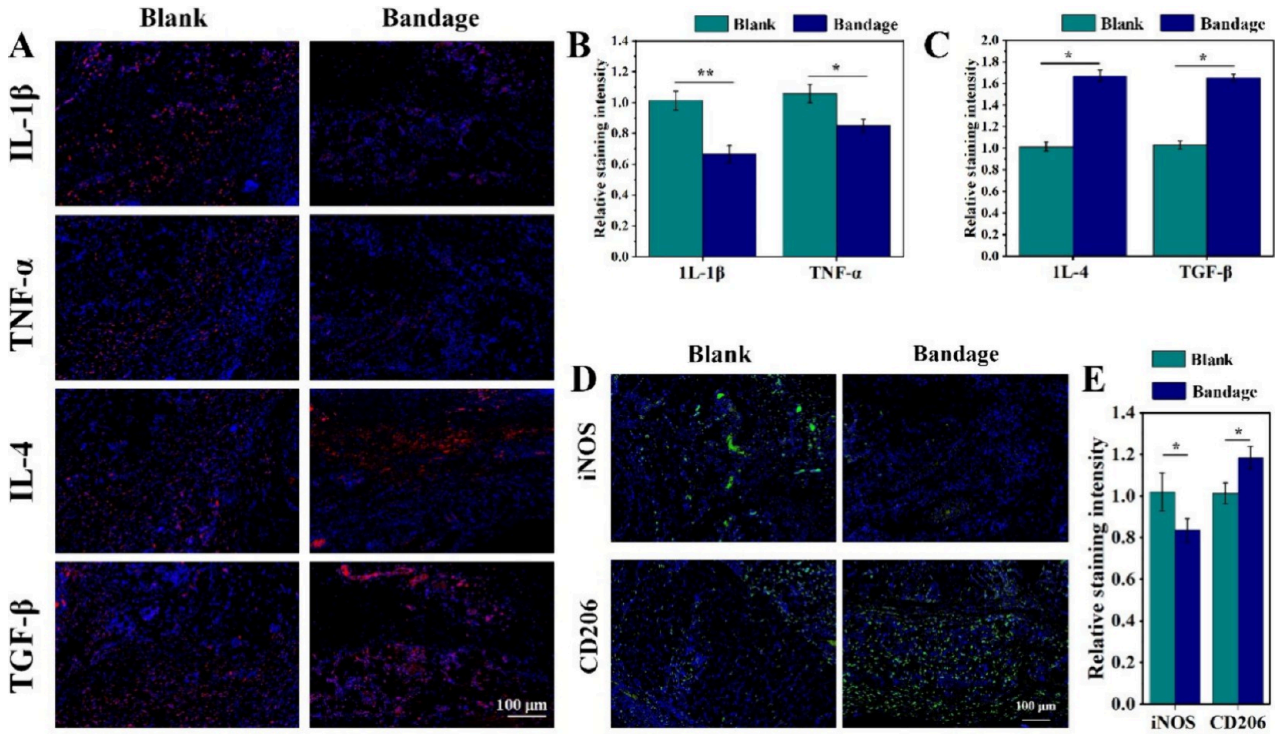

Figure 8. Immune microenvironment of wounds at the early stage. (A) Immunofluorescence staining of IL-1β, TNF-α, IL-4, and TGF-β1 on the wound samples on day 3 (bar scale: 100 μm). (B) Relative staining intensity of IL-1β and TNF-α (*p < 0.05, **p < 0.01). (C) Relative staining intensity of IL-4 and TGF-β1 (*p < 0.05). (D) Immunofluorescence staining of iNOS and CD206 (bar scale: 100 μm). (E) Relative staining intensity of iNOS and CD206 (*p < 0.05). n = 5.

endothelial cells, the positive expression of CD31 in the wound site in the Bandage group was higher than that in the Blank group on day 7, revealing that the hydrogel bandage had a positive effect on angiogenesis. After 14 days, the expression of CD31 in the Bandage group decreased significantly, indicating that the wound entered the period of vascular inhibition and remodeling. However, the strong expression of CD31in the Blank group indicated that the wound was in the repair stage (Figure 7F and Figure S18).

In addition, to study the related factors of hydrogel bandage promoting wound healing, the inflammatory microenvironment of the early stage of wounds on day 3 was evaluated. According to interleukin-1β (IL-1β), tumor necrosis factor-α (TNF-α), interleukin-4 (IL-4), and transforming growth factor-β1 (TGF-β1) immunofluorescence staining (Figure 8A−C), the lowest fluorescence intensity of IL-1β and TNF-α in the Bandage group illustrated that these pro-inflammatory factors were significantly inhibited, while the anti-inflammatory factor (IL-4) expression in the Bandage group was significantly higher than that in the Blank group, revealing that at the early stage of wound healing the hydrogel bandage promoted the secretion of anti-inflammatory factors and inhibited local inflammatory response to accelerate wound healing. At the same time, TGF-β1 was upregulated in the Bandage group. TGF-β1 plays an important role in mediating M1/M2 subtype transformation and the subsequent tissue repair and angiogenesis.[47] The upregulation of TGF-β1 promoted angiogenesis, which had been confirmed with the above CD31 immunofluorescence staining results. Meanwhile, to verify the transformation effect of the hydrogel bandage on macrophages in vivo, iNOS (M1 type macrophage marker) staining and CD206 (M2 type macrophage marker) immunofluorescence staining were performed. According to Figure 8D,E, it was found that in the Blank group, the iNOS expression was higher, while in the Bandage group, the CD206 expression was higher, indicating that the hydrogel bandage significantly affected the macrophage polarization, leading to more M2 macrophages. M2 macrophages mainly secrete high levels of anti-inflammatory cytokines and repair growth factors to promote tissue regeneration.[48] Thus, the CD31 immunofluorescence staining results, the pro-inflammatory and anti-inflammatory factors immunofluorescence staining results, and the macrophage marker immunofluorescence staining results illustrated that the application of hydrogel bandage provided an immune microenvironment conducive to tissue repair, thereby promoting wound healing.

4. CONCLUSION

In summary, this study reported a rapid gelation phenomenon of LA in water with the assistance of trometamol. The binary system of LA and tromtamol could quickly gel in water to form an injectable supramolecular hydrogel within 5 min. With the help of HALA and CNC, this hydrogel could realize 3D printing for producing PLA-based hydrogel bandages. HALA and CNC were found to exhibit a significant effect on stabilizing PLA by preventing PLA depolymerization. At the same time, HALA and CNC were employed as the macromolecular covalent cross-linker and the giant physical cross-linker to synergistically endow the hydrogel with higher cohesion, significantly improving the modulus and the toughness of the hydrogel. The adhesion strength of the hydrogel bandage PLA-HA-CNC5 reached to ∼134 kPa, which was ∼10 times higher than that of the clinically used FibrinGlue. The hydrogel bandage possessed a quick self-

https://doi.org/10.1021/acsami.4c11704
ACS Appl. Mater. Interfaces 2024, 16, 53515−53531

healing ability. After blasting, the bursting pressure of the healed hydrogel bandage reached 80%−95% of the original bursting pressure. Although the hydrogel bandage had strong adhesion, it could be removed without residue within 60 s by washing with water flowing. The in vivo healing of full-thickness wounds confirmed that the application of the bioadhesive hydrogel bandage significantly promoted wound healing by closing the wound, forming a physical barrier to the wound, and providing an anti-inflammatory effect. The preparation process of the hydrogel bandage did not need complex equipment as well as tedious and time-consuming post-treatment to ensure the reliable biocompatibility. Therefore, the present hydrogel bandage and its preparation methods have potential for future clinical applications.

■ ASSOCIATED CONTENT

Data Availability Statement

The data are available from the corresponding author upon reasonable request.

Supporting Information

The Supporting Information is available free of charge at https://pubs.acs.org/doi/10.1021/acsami.4c11704.

Figure S1: effect of composition on rapid gelation and mechanical properties, (A) effect of LA concentration and LA/Tris molar ratio on rapid gelation, (B) effect of LA concentration on G'; Figure S2: swelling of the rapidly gelled hydrogel in water; Figure S3: FT-IR spectrum of LA and Tris; Figure S4: G' of PLA polymerized form LA solution with the LA concentration of 50% w/v and the Tris concentration of 30% w/v during heating; Figure S5: characterization of HALA, (A) synthesis of HALA, (B) FT-IR spectrum, (C) UV−visible absorption spectrum, (D) ^{1}H NMR spectrum of HALA; Figure S6: molecular weight of HA before and after LA conjugation tested by GPC; Figure S7: characterization of CNC, (A) SEM image of CNC (bar scale = 100 μm), (B) size distribution of CNC in water; Figure S8: evaluation of printability, (A) effect of HALA concentration and CNC content on printability, (B) observation of the ink (LA: 50% w/v; trometamol: 30% w/v; HALA: 2% w/v; CNC: 5%) prepared from nonrapidly gelled system; Figure S9: effect of LA concentration on polymerization in water, (A) UV−visible absorption spectra, (B) normalized absorbance of LA concentration; Figure S10: statistics of the extruded filament diameter before and after 3 h heating; Figure S11: zeta potential of CNC and LA-CNC; Figure S12: microstructure of hydrogel bandage with and without CNC, (A) SEM images, (B) EDS images of hydrogel bandage with and without CNC; Figure S13: swelling behavior and swelling ratio of the bandage; Figure S14: bandage re-adhesion, (A) images to show the re-adhesion of the removed hydrogel bandage, (B) adhesion strength of the re-adhered hydrogel bandage; Figure S15: residual stress percentage of different hydrogels calculated from cyclic compression tests; Figure S16: pH value of the hydrogels; Figure S17: in vitro biocompatibility, (A) live/dead staining of fibroblasts co-cultured with hydrogel bandage (PLA-HA-CNC2) (bar scale = 50 μm), (B) OD value to show fibroblasts proliferated after 1, 5, and 7 days culture; Figure S18: relative CD31 staining intensity calculated by ImageJ; Table S1: DFT calculation results; Table S2: synthesis of HALA (PDF)

■ AUTHOR INFORMATION

Corresponding Authors

Huijie Gu − *Department of Orthopedics, Minhang Hospital, Fudan University, Shanghai 201199, P. R. China*; Email: guhuijie0110@126.com

Kunxi Zhang − *Department of Emergency, Tongji Hospital, School of Medicine, Tongji University, Shanghai 200065, P. R. China; Department of Polymer Materials, School of Materials Science and Engineering, Shanghai University, Shanghai 200444, P. R. China*; orcid.org/0000-0002-6341-3182; Email: zhangkunxi@shu.edu.cn

Yanli Song − *Department of Emergency, Tongji Hospital, School of Medicine, Tongji University, Shanghai 200065, P. R. China*; Email: songyanli@tongji.edu.cn

Authors

Jiujiang Zeng − *Department of Emergency, Tongji Hospital, School of Medicine, Tongji University, Shanghai 200065, P. R. China*

Haowei Fang − *Department of Polymer Materials, School of Materials Science and Engineering, Shanghai University, Shanghai 200444, P. R. China*

Haiyang Pan − *Department of Polymer Materials, School of Materials Science and Engineering, Shanghai University, Shanghai 200444, P. R. China*

Complete contact information is available at: https://pubs.acs.org/10.1021/acsami.4c11704

Funding

This research was supported by the National Natural Science Foundation of China (Grant No. 52373146), the Natural Science Foundation of Shanghai (Nos. 22ZR1424700, 22ZR1454900), and the Shanghai Tongji Hospital Incubation Project (No. GJPY2324).

Notes

The authors declare no competing financial interest.

■ REFERENCES

(1) O'neil, J.; Kovach, S. Xylazine-associated skin injury. *New. Engl. J. Med.* **2023**, *388*, 2274.

(2) Nakipoglu, M.; Tezcaner, A.; Contag, C. H.; Annabi, N.; Ashammakhi, N. Bioadhesives with antimicrobial properties. *Adv. Mater.* **2023**, *35*, 2300840.

(3) Taghizadeh, A.; Taghizadeh, M.; Yazdi, M. K.; Zarrintaj, P.; Ramsey, J. D.; Seidi, F.; Stadler, F. J.; Lee, H.; Saeb, M. R.; Mozafari, M. Mussel-inspired biomaterials: from chemistry to clinic. *Bioeng. Transl. Med.* **2022**, *7*, No. e10385.

(4) Chen, X.; Zhang, J.; Chen, G.; Xue, Y.; Zhang, J.; Liang, X.; Lei, I. M.; Lin, J.; Xu, B. B.; Liu, J. Hydrogel bioadhesives with extreme acid-tolerance for gastric perforation repairing. *Adv. Funct. Mater.* **2022**, *32*, 2202285.

(5) Ma, Y.; Yao, J.; Liu, Q.; Han, T.; Zhao, J.; Ma, X.; Tong, Y.; Jin, G.; Qu, K.; Li, B.; Xu, F. Liquid bandage harvests robust adhesive, hemostatic, and antibacterial performances as a first-aid tissue adhesive. *Adv. Funct. Mater.* **2020**, *30*, 2001820.

(6) Liang, Y.; He, J.; Guo, B. Functional hydrogels as wound dressing to enhance wound healing. *ACS Nano* **2021**, *15*, 12687.

(7) Wang, L.; Zhou, M.; Xu, T.; Zhang, X. Multifunctional hydrogel as wound dressing for intelligent wound monitoring. *Chem. Eng. J.* **2022**, *433*, 134625.

(8) Rao, P.; Sun, T. L.; Chen, L.; Takahashi, R.; Shinohara, G.; Guo, H.; King, D. R.; Kurokawa, T.; Gong, J. P. Tough hydrogels with fast, strong, and reversible underwater adhesion based on a multiscale design. *Adv. Mater.* **2018**, *30*, 1801884.
(9) Han, Z.; Wang, P.; Lu, Y.; Jia, Z.; Qu, S.; Yang, W. A versatile hydrogel network-repairing strategy achieved by the covalent-like hydrogen bond interaction. *Sci. Adv.* **2022**, *8*, No. eabl5066.
(10) Fan, H.; Wang, J.; Tao, Z.; Huang, J.; Rao, P.; Kurokawa, T.; Gong, J. Adjacent cationic-aromatic sequences yield strong electrostatic adhesion of hydrogels in seawater. *Nat. Commun.* **2019**, *10*, 5127.
(11) Xu, X.; Jerca, V. V.; Hoogenboom, R. Bioinspired double network hydrogels: from covalent double network hydrogels via hybrid double network hydrogels to physical double network hydrogels. *Mater. Horiz.* **2021**, *8*, 1173.
(12) Xue, B.; Gu, J.; Li, L.; Yu, W.; Yin, S.; Qin, M.; Jiang, Q.; Wang, W.; Cao, Y. Hydrogel tapes for fault-tolerant strong wet adhesion. *Nat. Commun.* **2021**, *12*, 7156.
(13) Shui, L.; Jia, L.; Li, H.; Guo, J.; Guo, Z.; Liu, Y.; Liu, Z.; Chen, X. Rapid and continuous regulating adhesion strength by mechanical micro-vibration. *Nat. Commun.* **2020**, *11*, 1583.
(14) Li, M.; Pan, G.; Yang, Y.; Guo, B. Smart aligned multi-layered conductive cryogels with hemostasis and breathability for coagulopathy epistaxis, nasal mucosal repair and bleeding monitoring. *Nano Today* **2023**, *48*, 101720.
(15) Guo, B.; Dong, R.; Liang, Y.; Li, M. Haemostatic materials for wound healing applications. *Nat. Rev. Chem.* **2021**, *5*, 773−791.
(16) Wang, L.; Jing, P.; Tan, J.; Liao, C.; Chen, Y.; Yu, Y.; Zhang, S. One-stitch" bioorthogonal prodrug activation based on cross-linked lipoic acid nanocapsules. *Biomaterials* **2021**, *273*, 120823.
(17) Sakai, N.; Lista, M.; Kel, O.; Sakurai, S.; Emery, D.; Mareda, J.; Vauthey, E.; Matile, S. Self-organizing surface-initiated polymerization: Facile access to complex functional systems. *J. Am. Chem. Soc.* **2011**, *133*, 15224−15227.
(18) Zhang, X.; Waymouth, R. M. 1,2-Dithiolane-derived dynamic, covalent materials: Cooperative self-assembly and reversible cross-linking. *J. Am. Chem. Soc.* **2017**, *139*, 3822−3833.
(19) Deng, Y.; Zhang, Q.; Shi, C.; Toyoda, R.; Qu, D.; Tian, H.; Feringa, B. Acylhydrazine-based reticular hydrogen bonds enable robust, tough, and dynamic supramolecular materials. *Sci. Adv.* **2022**, *8*, abk3286.
(20) Gao, J.; Zhang, Q.; Wu, B.; Gao, X.; Liu, Z.; Yang, H.; Yuan, J.; Huang, J. Mussel-inspired, underwater self-healing ionoelastomers based on α-lipoic acid for iontronics. *Small* **2023**, *19*, 2207334.
(21) Cui, C.; Sun, Y.; Nie, X.; Yang, X.; Wang, F.; Liu, W. A coenzyme-based deep eutectic supramolecular polymer bioadhesive. *Adv. Funct. Mater.* **2023**, *33*, 2307543.
(22) Zhang, Q.; Shi, C. Y.; Qu, D. H.; Long, Y. T.; Feringa, B. L.; Tian, H. Exploring a naturally tailored small molecule for stretchable, self-healing, and adhesive supramolecular polymers. *Sci. Adv.* **2018**, *4*, No. eaat8192.
(23) Ke, X.; Tang, S.; Dong, Z.; Ren, K.; Yu, P.; Xu, X.; Yang, J.; Luo, J.; Li, J. An instant, repeatable and universal supramolecular adhesive based on natural small molecules for dry/wet environments. *Chem. Eng. J.* **2022**, *442*, 136206.
(24) Huang, H.; Wang, H.; Sun, L.; Zhang, R.; Zhang, L.; Wu, Z.; Zheng, Y.; Wang, Y.; Fu, W.; Zhang, Y.; Neisiany, R. E.; You, Z. Long-range electronic effect-promoted ring-opening polymerization of thioctic acid to produce biomimetic ionic elastomers for bioelectronics. *CCS Chem.* **2024**, *6*, 761−773.
(25) Zhu, J.; Zhao, S.; Luo, J.; Niu, W.; Damron, J. T.; Zhang, Z.; Rahman, M. A.; Arnould, M. A.; Saito, T.; Advincula, R.; Sokolov, A. P.; Sumpter, B. G.; Cao, P. F. A novel dynamic polymer synthesis via chlorinated solvent quenched depolymerization. *CCS Chem.* **2023**, *5*, 1841−1853.
(26) Cai, C.; Wu, S.; Zhang, Y.; Li, F.; Tan, Z.; Dong, S. Poly(thioctic acid): from bottom-up self-assembly to 3D-fused deposition modeling printing. *Adv. Sci.* **2022**, *9*, 2203630.
(27) Machado, T. O.; Stubbs, C. J.; Chiaradia, V.; Alraddadi, M. A.; Brandolese, A.; Worch, J. C.; Dove, A. P. A renewably sourced, circular photopolymer resin for additive manufacturing. *Nature* **2024**, *629*, 1069−1074.
(28) Fang, Z.; Mu, H.; Sun, Z.; Zhang, K.; Zhang, A.; Chen, J.; Zheng, N.; Zhao, Q.; Yang, X.; Liu, F.; Wu, J.; Xie, T. 3D printable elastomers with exceptional strength and toughness. *Nature* **2024**, *631*, 783−788.
(29) Deng, Y.; Zhang, Q.; Feringa, B. L.; Tian, H.; Qu, D. H. Toughening a self-healable supramolecular polymer by ionic cluster-enhanced iron-carboxylate complexes. *Angew. Chem., Int. Ed.* **2020**, *59*, 5278−5283.
(30) Wang, Y.; Sun, S.; Wu, P. Adaptive ionogel paint from room-temperature autonomous polymerization of α-thioctic acid for stretchable and healable electronics. *Adv. Funct. Mater.* **2021**, *31*, 2101494.
(31) Chen, C.; Yang, X.; Li, S. J.; Zhang, C.; Ma, Y. N.; Ma, Y. X.; Gao, P.; Gao, S. Z.; Huang, X. J. Tannic acid-thioctic acid hydrogel: a novel injectable supramolecular adhesive gel for wound healing. *Green Chem.* **2021**, *23*, 1794−1804.
(32) Yang, X.; Zhang, B.; Li, J.; Shen, M.; Liu, H.; Xu, X.; Shang, S. Self-healing, self-adhesive, and stretchable conductive hydrogel for multifunctional sensor prepared by catechol modified nanocellulose stabilized poly(α-thioctic acid). *Carbohydr. Polym.* **2023**, *313*, 120813.
(33) Xie, T.; Ding, J.; Han, X.; Jia, H.; Yang, Y.; Liang, S.; Wang, W.; Liu, W.; Wang, W. Wound dressing change facilitated by spraying zinc ions. *Mater. Horiz.* **2020**, *7*, 605−614.
(34) Neese, F. Software update: The ORCA program system—Version 5.0. *WIREs Comput. Mol. Sci.* **2022**, *12*, No. e1606.
(35) Neese, F. An improvement of the resolution of the identity approximation for the formation of the Coulomb matrix. *J. Comput. Chem.* **2003**, *24*, 1740−1747.
(36) Neese, F.; Wennmohs, F.; Hansen, A.; Becker, U. Efficient, approximate and parallel Hartree-Fock and hybrid DFT calculations. A'chain-of-spheres' algorithm for the Hartree-Fock exchange. *Chem. Phys.* **2009**, *356*, 98−109.
(37) Neese, F. The SHARK integral generation and digestion system. *J. Comput. Chem.* **2023**, *44*, 381−396.
(38) Grimme, S.; Antony, J.; Ehrlich, S.; Krieg, H. A consistent and accurate ab initio parametrization of density functional dispersion correction (DFT-D) for the 94 elements H-Pu. *J. Chem. Phys.* **2010**, *132*, 154104.
(39) Grimme, S.; Ehrlich, S.; Goerigk, L. Effect of the damping function in dispersion corrected density functional theory. *J. Comput. Chem.* **2011**, *32*, 1456−1465.
(40) Zhang, S.; Pan, Y.; Mao, Z.; Zhang, J.; Zhang, K.; Yin, J.; Wang, C. Hyaluronic acid-g-lipoic acid granular gel for promoting diabetic wound healing. *Bioeng. Transl. Med.* **2023**, *8*, No. e10402.
(41) Zhang, Q.; Deng, Y. X.; Luo, H. X.; Shi, C. Y.; Geise, G. M.; Feringa, B. L.; Tian, H.; Qu, D. H. Assembling a natural small molecule into a supramolecular network with high structural order and dynamic functions. *J. Am. Chem. Soc.* **2019**, *141*, 12804−12814.
(42) Zhang, Q.; Qu, D. H.; Feringa, B. L.; Tian, H. Disulfide-Mediated reversible polymerization toward intrinsically dynamic smart materials. *J. Am. Chem. Soc.* **2022**, *144*, 2022−2033.
(43) Liu, Z.; Yan, F. Switchable adhesion: on-demand bonding and debonding. *Adv. Sci.* **2022**, *9*, 2200264.
(44) Kong, X.; Jin, X.; Xiao, M.; Yang, J.; Zou, Y.; Xie, X.; Liu, C.; Wei, X.; Yang, J.; Wang, W. An extensively adhesive patch with multiple physical interactions and chemical crosslinking as a wound dressing and strain sensor. *ACS Appl. Mater. Interfaces* **2022**, *4*, 3926−3941.
(45) Kim, H.; Choi, S.; Hong, Y.; Chung, J.; Choi, J.; Choi, W. K.; Park, I. W.; Park, S. H.; Park, H.; Chung, W. J.; Heo, K.; Lee, M. Biocompatible and biodegradable triboelectric nanogenerators based on hyaluronic acid hydrogel film. *Appl. Mater. Today* **2021**, *22*, 100920.

https://doi.org/10.1021/acsami.4c11704
ACS Appl. Mater. Interfaces 2024, 16, 53515−53531

(46) Zeng, J.; Chen, X.; Zhang, J.; Qin, Y.; Zhang, K.; Li, X.; Cui, H. Stem cell spheroids production for wound healing with a reversible porous hydrogel. *Mater. Today Adv.* **2022**, *15*, 100269.
(47) Zhou, L.; Liu, N.; Feng, L.; Zhao, M.; Wu, P.; Chai, Y.; Liu, J.; Zhu, P.; Guo, R. Multifunctional electrospun asymmetric wettable membrane containing black phosphorus/Rg1 for enhancing infected wound healing. *Bioeng. Transl. Med.* **2022**, *7*, No. e10274.
(48) Wu, W. K.; Llewellyn, O. P. C.; Bates, D. O.; Nicholson, L. B.; Dick, A. D. IL-10 regulation of macrophage VEGF production is dependent on macrophage polarisation and hypoxia. *Immunobiology* **2010**, *215*, 796−803.

https://doi.org/10.1021/acsami.4c11704
ACS Appl. Mater. Interfaces 2024, 16, 53515−53531